JBC RESEARCH ARTICLE

UGT86C11 is a novel plant UDP-glycosyltransferase involved in labdane diterpene biosynthesis

Received for publication, March 25, 2021, and in revised form, July 28, 2021 Published, Papers in Press, August 4, 2021,
https://doi.org/10.1016/j.jbc.2021.101045

Payal Srivastava[1,2], **Anchal Garg**[1], **Rajesh Chandra Misra**[1], **Chandan Singh Chanotiya**[3], **and Sumit Ghosh**[1,2,*]

From the [1]*Plant Biotechnology Division, Council of Scientific and Industrial Research-Central Institute of Medicinal and Aromatic Plants (CSIR-CIMAP), Lucknow, India;* [2]*Academy of Scientific and Innovative Research (AcSIR), Ghaziabad, India; and* [3]*Phytochemistry Division, Council of Scientific and Industrial Research-Central Institute of Medicinal and Aromatic Plants (CSIR-CIMAP), Lucknow, India*

Edited by Gerald Hart

Glycosyltransferases constitute a large family of enzymes across all domains of life, but knowledge of their biochemical function remains largely incomplete, particularly in the context of plant specialized metabolism. The labdane diterpenes represent a large class of phytochemicals with many pharmacological benefits, such as anti-inflammatory, hepatoprotective, and anticarcinogenic. The medicinal plant kalmegh (*Andrographis paniculata*) produces bioactive labdane diterpenes; notably, the C19-hydroxyl diterpene (andrograpanin) is predominantly found as C19-O-glucoside (neoandrographolide), whereas diterpenes having additional hydroxylation(s) at C3 (14-deoxy-11,12-didehydroandrographolide) or C3 and C14 (andrographolide) are primarily detected as aglycones, signifying scaffold-selective C19-O-glucosylation of diterpenes *in planta*. Here, we analyzed UDP-glycosyltransferase (UGT) activity and diterpene levels across various developmental stages and tissues and found an apparent correlation of UGT activity with the spatiotemporal accumulation of neoandrographolide, the major diterpene C19-O-glucoside. The biochemical analysis of recombinant UGTs preferentially expressed in neoandrographolide-accumulating tissues identified a previously uncharacterized UGT86 member (ApUGT12/UGT86C11) that catalyzes C19-O-glucosylation of diterpenes with strict scaffold selectivity. ApUGT12 localized to the cytoplasm and catalyzed diterpene C19-O-glucosylation *in planta*. The substrate selectivity demonstrated by the recombinant ApUGT12 expressed in plant and bacterium hosts was comparable to native UGT activity. Recombinant ApUGT12 showed significantly higher catalytic efficiency using andrograpanin compared with 14-deoxy-11,12-didehydroandrographolide and trivial activity using andrographolide. Moreover, *ApUGT12* silencing in plants led to a drastic reduction in neoandrographolide content and increased levels of andrograpanin. These data suggest the involvement of ApUGT12 in scaffold-selective C19-O-glucosylation of labdane diterpenes in plants. This knowledge of UGT86 function might help in developing plant chemotypes and synthesis of pharmacologically relevant diterpenes.

Plants make an astonishing diversity of chemicals that are important to their overall fitness in a challenging environment and are also valuable as pharmaceuticals and various industrial chemicals (1–3). The diversity in plant specialized pathway is believed to have originated because of the evolution of diverse enzyme function following gene duplication and neo-functionalization (4). A genome-wide analysis found about 15% of the protein-coding genes corresponds to the specialized metabolic pathways in plants (5). Besides, the enzymes of the plant specialized metabolism often show catalytic promiscuity, leading to additional product diversity. The glycosyltransferases (GTs) detected in all forms of life catalyze the transfer of sugar moiety from activated sugar donors (*e.g.*, nucleotide diphosphate/monophosphate sugar or lipid phosphate sugar) to various acceptor molecules, such as nucleotides, sugars, lipids, proteins, antibiotics, and small molecules/specialized metabolites (6, 7). In the Carbohydrate-Active enZYmes database, the multigene family GTs are broadly classified into 114 families depending on sequence similarity (http://www.cazy.org/GlycosylTransferases.html). The GTs involved in glycosylation of small molecules such as plant specialized metabolites are grouped under the GT1 family, representing the largest GT family in plants. For example, GT1 family represents more than 25% to 35% GTs in model plants, Arabidopsis and rice (7). GT1 are also referred to as UDP-glycosyltransferases (UGTs) considering that they utilize UDP-sugar as sugar donor. In majority of cases, plant UGTs utilize UDP-glucose as sugar donor, although UDP-galactose, UDP-xylose, UDP-rhamnose, and UDP-glucuronic acid are also accepted by some UGTs (8–10).

Plant UGTs have been the subject of immense interest owing to their important roles in the biosynthesis of pharmaceutically relevant phytochemicals, regulation of cellular homeostasis, and detoxification of xenobiotics (7, 10–16). The glycosylation most often represents a final step in the biosynthesis of phytochemicals, thereby, influencing their solubility, storage, and bioactivity (17–19). Consequently, understanding the biochemical features of UGTs will be essential to engineer bioactive chemicals in plants to improve plant function and provide benefits to human health (14, 20–24). However, considering a huge diversity of UGTs even in a

* For correspondence: Sumit Ghosh, sumitg80@gmail.com, sumitghosh@cimap.res.in.
Present address for Rajesh Chandra Misra: Biochemistry and Metabolism Department, John Innes Centre, Norwich, United Kingdom.

single plant species and the diversity of specialized metabolites produced in plants, it is quite impossible to assign biochemical function of UGTs in plant specialized metabolism, solely based on sequence similarity. For example, Arabidopsis and rice encode about 120 and 215 UGTs, respectively, but only about 25% UGTs are biochemically characterized so far, and the native substrates of many of the UGTs remain to be known (7, 25, 26).

The labdane diterpenes form a large family of phytochemicals with a broad range of bioactivities (27). These diterpenes represent a major group of bioactive chemicals in the medicinal plant kalmegh (*Andrographis paniculata*) (28–32). Neoandrographolide, a major bioactive diterpene C19-O-glucoside in kalmegh, possesses anti-inflammatory, hepatoprotective, anticarcinogenic, hypolipidemic, and viricidal activities (33–37). In some studies, neoandrographolide showed superior bioactivity than the diterpene aglycones andrographolide and 14-deoxy-11,12-didehydroandrographolide, suggesting a possible role of glucosylation toward enhanced bioactivity and/or bioavailability of neoandrographolide (33, 37–39). Neoandrographolide biosynthesis in kalmegh starts with a diterpene cyclization reaction catalyzed by the diterpene synthase, converting a general diterpene precursor geranylgeranyl pyrophosphate to ent-copalyl pyrophosphate (Fig. 1). Previously, we have identified a diterpene synthase (ApCPS2) catalyzing the first committed reaction in the neoandrographolide biosynthetic pathway (40, 41). The final step in neoandrographolide biosynthesis involves C19-O-glucosylation of andrograpanin (Fig. 1). However, UGT involved in developmental and tissue-specific biosynthesis of neoandrographolide was not identified. Previously, two methyl jasmonate (MeJA)–inducible UGTs (UGT73AU1 and UGT5), which catalyzed *in vitro* C19-O-glucosylation of andrograpanin, were identified, but their involvement *in planta* biosynthesis of neoandrographolide was not understood (42, 43). To investigate the UGT involved in spatiotemporal biosynthesis of neoandrographolide, we have analyzed a large-scale transcriptome data of kalmegh and identified UGTs that preferentially expressed in neoandrographolide-accumulating tissues. Furthermore, 23 recombinant UGTs were screened in UGT assay, leading to the identification of ApUGT12 (UGT86C11) catalyzing C19-O-glucosylation of diterpenes in a scaffold-selective manner (Fig. 1). The steady-state kinetic of ApUGT12, an altered diterpene profiles in *ApUGT12*-silenced plants, and a strong correlation of *ApUGT12* transcript expression with UGT activity and neoandrographolide accumulation patterns across various developmental stages and tissues suggested a pivotal role of ApUGT12 in the biosynthesis of diterpene C19-O-glucoside.

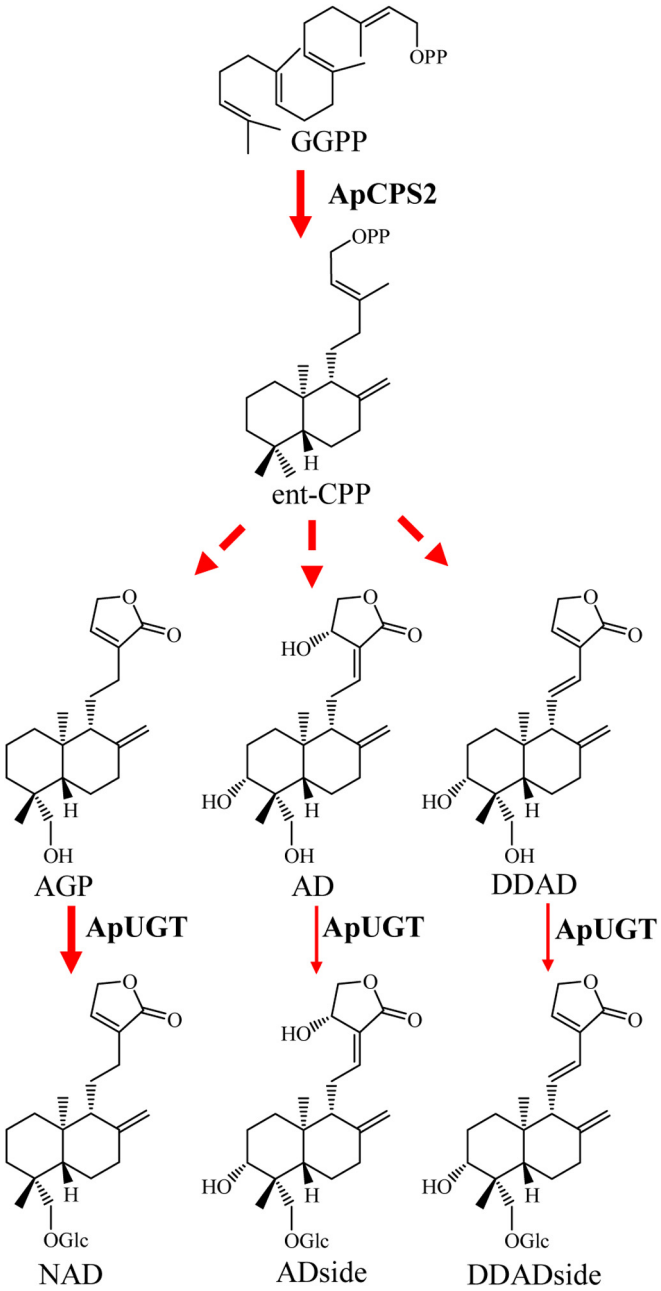

Figure 1. A proposed pathway for ent-labdane–related diterpene biosynthesis in kalmegh. Andrographolide (AD) and 14-deoxy-11,12-didehydroandrographolide (DDAD) are the major diterpene aglycones found in kalmegh tissues, whereas neoandrographolide (NAD) is the major diterpene C19-O-glucoside. Andrograpanin (AGP), andrographiside (ADside), and 14-deoxy-11,12-didehydroandrographiside (DDADside) are detected in trace levels in kalmegh tissues. *Thin arrows* represent biochemical reactions that might work inefficiently *in planta*. *Dashed arrows* mark multiple uncharacterized biochemical steps. ApCPS2 is a previously characterized diterpene synthase converting geranylgeranyl pyrophosphate (GGPP) to ent-copalyl pyrophosphate (ent-CPP). Scaffold-selective C19-O-glucosylation by UDP-glycosyltransferase (ApUGT) potentially determines selective accumulation of diterpene aglycones and glucosides in kalmegh.

Results

Developmental and tissue-specific patterns of diterpene C19-O-glucosylation activity

To understand spatiotemporal biosynthesis of diterpenes, we conducted comprehensive profiling of diterpene aglycones (andrographolide, andrograpanin, and 14-deoxy-11,12-didehydroandrographolide) and diterpene C19-O-glucosides (neoandrographolide, andrographiside, and 14-deoxy-11,12-didehydroandrographiside) across five developmental stages (germinating seeds, cotyledonary leaf stage, 15-day-old plants, 30-day-old plants, and 60-day-old plants) using six tissues (root, leaf,

stem, sepal, petal, and seedpod) (Fig. S1). HPLC analysis of methanolic extracts revealed higher content of neoandrographolide, andrographolide, and 14-deoxy-11,12-didehydroandrographolide in leaves (Figs. 2*A*, S2, and S3, *A* and *B*). However, these diterpenes were not detected in roots and germinating seeds. In addition, neoandrographolide, andrographolide, and 14-deoxy-11,12-didehydroandrographolide were also detected in considerable amounts in seedpod, sepal, and cotyledonary leaf stage seedlings, respectively. The increased amount of neoandrographolide than andrograpanin in kalmegh tissues suggested ready conversion of andrograpanin to neoandrographolide following C19-O-glucosylation, thus limiting *in planta* accumulation of andrograpanin (Figs. 1 and 2*A*). On the other hand, higher content of andrographolide and 14-deoxy-11,12-didehydroandrographolide than the corresponding C19-O-glucosides (andrographiside and 14-deoxy-11,12-dide hydroandrographiside) indicated inefficient C19-O-glucosylation of andrographolide and 14-deoxy-11,12-didehydroandrographolide (Figs. 1 and S3, *A* and *B*). These results suggest that scaffold-selective C19-O-glucosylation potentially contributes to distinct patterns of diterpene aglycones and glucosides *in planta*. To investigate the involvement of UGT in diterpene C19-O-glucosylation, UGT assays were carried out using total protein extract of various tissues. Andrograpanin, andrographolide, and 14-deoxy-11,12-didehydroandrographolide were the sugar acceptors, whereas UDP-glucose served as sugar donor in assays. Diterpene C19-O-glucoside produced in assay was monitored by HPLC. UGT assays using andrograpanin as sugar acceptor revealed considerably higher enzyme activity in leaves of 60-day-old and 30-day-old plants followed by in leaves of 15-day-old plants and seedpod (Fig. 2*B*). These tissues also contained higher amount of neoandrographolide (Fig. 2*A*). UGT assay using total protein extract of roots and germinating seeds could not form neoandrographolide. Likewise, neoandrographolide was not detected in roots and germinating seeds. In contrast, UGT assay using 14-deoxy-11,12-didehydroandrographolide revealed considerably lower activity than using andrograpanin (Fig. S4). However, C19-O-glucosylation of andrographolide could not be achieved at a detectable level using total protein extract of various tissues. Thus, higher UGT activity using andrograpanin than andrographolide and 14-deoxy-11,12-didehydroandrographolide might have contributed to neoandrographolide biosynthesis at a higher rate than andrographiside and 14-deoxy-11,12-didehydroandrographiside biosynthesis, leading to distinct profiles of diterpene aglycones and C19-O-glucosides *in planta* (Figs. 2, *A* and *B*, S3, *A* and *B*, and S4). Unlike andrograpanin, the other two diterpene aglycones (andrographolide and 14-deoxy-11,12-didehydroandrographolide) bear additional hydroxyl group(s) at the C3 and/or C14 positions. Therefore, these results strongly suggest that scaffold-selective C19-O-glucosylation of diterpene aglycones by UGT potentially contributes to selective accumulation of diterpene aglycones and glucosides.

Identification of candidate UGT of the diterpene pathway

Andrograpanin C19-O-glucosylation activity and neoandrographolide level in various tissues showed a clear correlation (Fig. 2, *A* and *B*). The maximum UGT activity toward andrograpanin C19-O-glucosylation was noticed in leaves of 60-day-old plants; however, UGT activity was not detected in roots. Similarly, neoandrographolide was detected at a higher level in leaves of 60-day-old plants, whereas neoandrographolide could not be detected in roots. To investigate

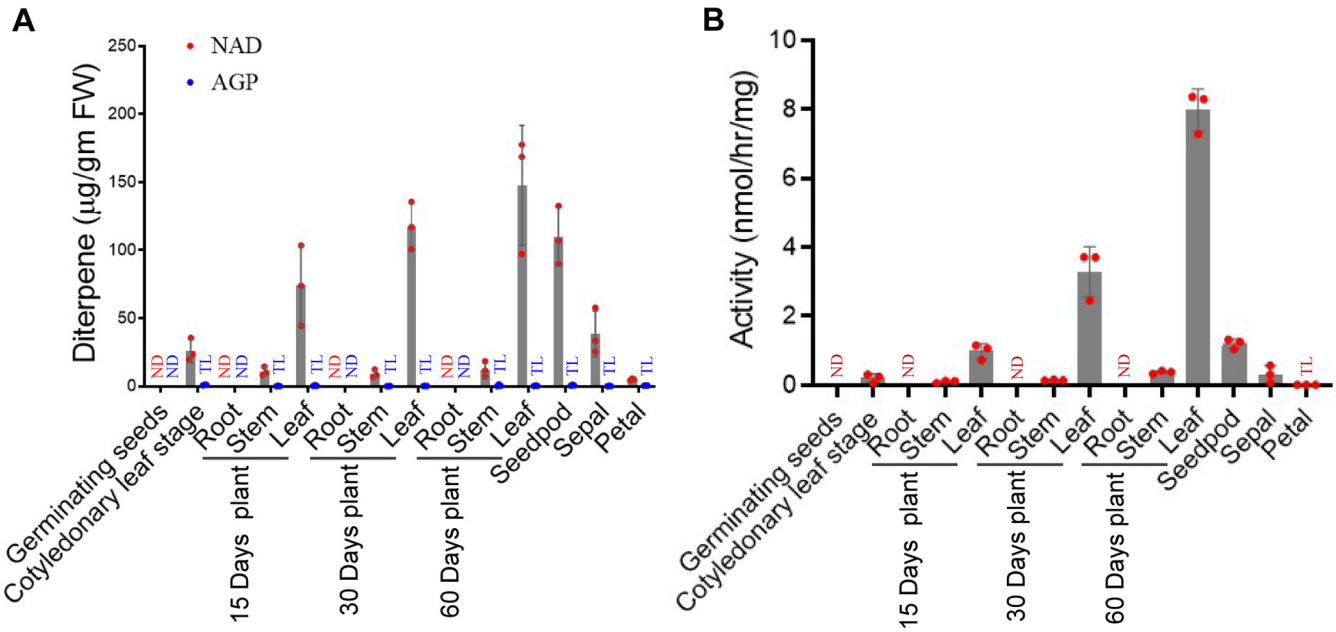

Figure 2. Spatiotemporal patterns of UGT activity and diterpene C19-O-glucoside accumulation. *A*, the content of neoandrographolide (NAD), the major diterpene C19-O-glucoside, and its precursor andrograpanin (AGP) in various tissues as determined by HPLC analysis of methanolic extracts. *B*, the pattern of UGT activity in various tissues. *In vitro* UGT assays were done in 10 mM Tris–Cl, pH 7.5, at 30 °C using andrograpanin (100 µM) and UDP-glucose (800 µM). The UGT activity is presented as the rate of neoandrographolide formation in assays using total protein extracts of various tissues. *A* and *B*, the data are means ± SD of three biological replicates. FW, fresh weight; ND, not detected; TL, trace level; UGT, UDP-glycosyltransferase.

the enzyme involved in C19-O-glucosylation of diterpenes, a large-scale RNA-Seq data representing more than 170 million sequencing reads of leaves and roots were screened and UGTs that preferentially expressed in leaves were identified (41). The transcripts potentially encoding UGTs were retrieved based on annotation to the Carbohydrate-Active enZYymes database following BlastX analysis. Among a total of 615 transcripts annotated to various GT families, 161 transcripts were categorized under the GT1/UGT family. Notably, *UGT73AU1* (contig ApU2595) and *UGT5* (contig ApU62177) transcript expression in leaves and roots was quite comparable (Fig. S5*A*). The previous study also found a similar transcript expression of *UGT73AU1* in leaves and roots; however, *UGT5* transcript expression in different tissues was not examined before (42, 43). To know whether UGT73AU1 and UGT5 contribute to developmental and tissue-specific C19-O-glucosylation of diterpenes, *UGT73AU1* and *UGT5* transcript expression was determined by quantitative RT-PCR (qRT-PCR) analysis and correlated with diterpene accumulation patterns and UGT activity (Fig. S6*A*). *UGT73AU1* and *UGT5* transcripts expressed at a higher level in roots of 60-day-old plants and sepal. However, andrograpanin C19-O-glucosylation activity and neoandrographolide content in these tissues were substantially lower or not detected (Fig. 2, *A* and *B*). Therefore, *UGT73AU1* and *UGT5* transcript expression patterns strongly indicated that they might not be playing a major role in developmental and tissue-specific biosynthesis of diterpene glucosides. Moreover, a similar catalytic efficiency of recombinant UGT5 using andrograpanin, andrographolide, and 14-deoxy-11,12-didehydroandrographolide could not corroborate differential activity of native UGT using these diterpene aglycones, if UGT5 is considered to be playing a major role *in planta* diterpene C19-O-glucosylation (Fig. S4) (42). The transcript expression of *ApCPS2*, which catalyzed the initial diterpene cyclization reaction in the neoandrographolide biosynthetic pathway, showed a strong correlation with developmental and tissue-specific biosynthesis of neoandrographolide (40, 41). Therefore, it could be hypothesized that UGT transcript expression might also coincide with *in planta* biosynthesis of neoandrographolide.

The analysis of RNA-Seq data identified 38 nonredundant UGT transcripts that expressed at a higher level in neoandrographolide-accumulating leaves than in roots (Fig. S5*A* and Table S1). To extract full-length coding sequences of the transcripts, transcriptome assemblies generated in other studies were also consulted (https://medplantrnaseq.org/) (44). Five transcripts that either represented incomplete ORFs or encoded truncated proteins were not considered thereafter (Table S1). Furthermore, the analysis of structural motifs in protein sequences identified 32 UGTs that contained the conserved 44 amino acids long plant secondary product glycosyltransferase motif, which participates in binding of UDP-sugar to the active site of *bona fide* UGTs (Figs. S5*B* and S7) (45). Although UGTs of the diterpene pathway were not well studied, some UGTs that participate in phenylpropanoid, sterol, and phytohormone pathways were previously characterized (10, 18, 20, 21, 25, 26, 46–48). To shortlist candidate UGTs of kalmegh diterpene pathway, a phylogenetic analysis was carried out using biochemically characterized UGTs. The analysis revealed 24 UGTs, which are not closely related with well-known UGTs of phenylpropanoid, sterol, and phytohormone pathways (Fig. S8). These UGTs were further considered for biochemical characterization to know their involvement in diterpene glucosylation.

ApUGT12 catalyzes diterpene C19-O-glucosylation

Among the selected UGTs, the complete ORF of 23 UGTs could be amplified using leaf complementary DNA (cDNA) as template and cloned in pET28a(+) vector for the expression of N-terminally 6×His-tagged recombinant proteins in *Escherichia coli*. To examine these UGTs for diterpene C19-O-glucosylation activity, *in vitro* assays were carried out using UDP-glucose as sugar donor whereas andrograpanin, andrographolide, and 14-deoxy-11,12-didehydroandrographolide as the sugar acceptors. To begin with, total protein extract of *E. coli* expressing recombinant UGTs and enriched fractions of recombinant UGTs (prepared following nickel–nitrilotriacetic acid [Ni–NTA] affinity chromatography) were used in UGT assays with andrograpanin as sugar acceptor. TLC and HPLC analysis of assay products revealed that only ApU56292 (thereafter described as ApUGT12) catalyzed C19-O-glucosylation of andrograpanin to form neoandrographolide (Fig. S9, *A* and *B*). To confirm this result, ApUGT12 was purified to electrophoretic homogeneity following Ni–NTA affinity chromatography, representing a ∼55 kDa protein band in 10% SDS-PAGE (Fig. 3*A*). The observed molecular mass of ApUGT12 was similar to the calculated molecular mass (57.99 kDa) of the recombinant ApUGT12. Furthermore, UGT assay was repeated using purified ApUGT12, andrograpanin, and UDP-glucose. The assay product analyzed by LC quadrupole TOF MS (LC–QTOF–MS) confirmed C19-O-glucosylation of andrograpanin to form neoandrographolide (Fig. 4, *A* and *B*). The QTOF mass spectrum of neoandrographolide formed in ApUGT12 assay was in accordance to the observed mass spectrum of neoandrographolide standard (Figs. 4*B* and S10). Besides, the recombinant ApUGT12 also catalyzed C19-O-glucosylation of 14-deoxy-11,12-didehydroandrographolide to produce 14-deoxy-11,12-didehydroandrographiside, which was identified based on mass spectrum data in LC–QTOF–MS analysis (Fig. S11, *A* and *B*). Notably, ApUGT12 showed considerably higher activity using andrograpanin than 14-deoxy-11,12-didehydroandrographolide (Fig. 3*D*). On the other hand, ApUGT12 exhibited trace activity using andrographolide as sugar acceptor (Figs. 3*D* and S12, *A* and *B*). The optimum pH and temperature for recombinant ApUGT12 were determined *in vitro* assays in a range of pH (pH 4.5–10) and temperatures (20–50 °C) using andrograpanin substrate (Fig. 3, *B* and *C*). The analysis revealed that pH 7.5 and 35 °C are the optimum pH and temperature for ApUGT12 activity. Taken together, these results confirmed that ApUGT12 catalyzes C19-O-glucosylation of andrograpanin, 14-deoxy-11,12-didehydroandrographolide, and andrographolide, although at a variable efficiency.

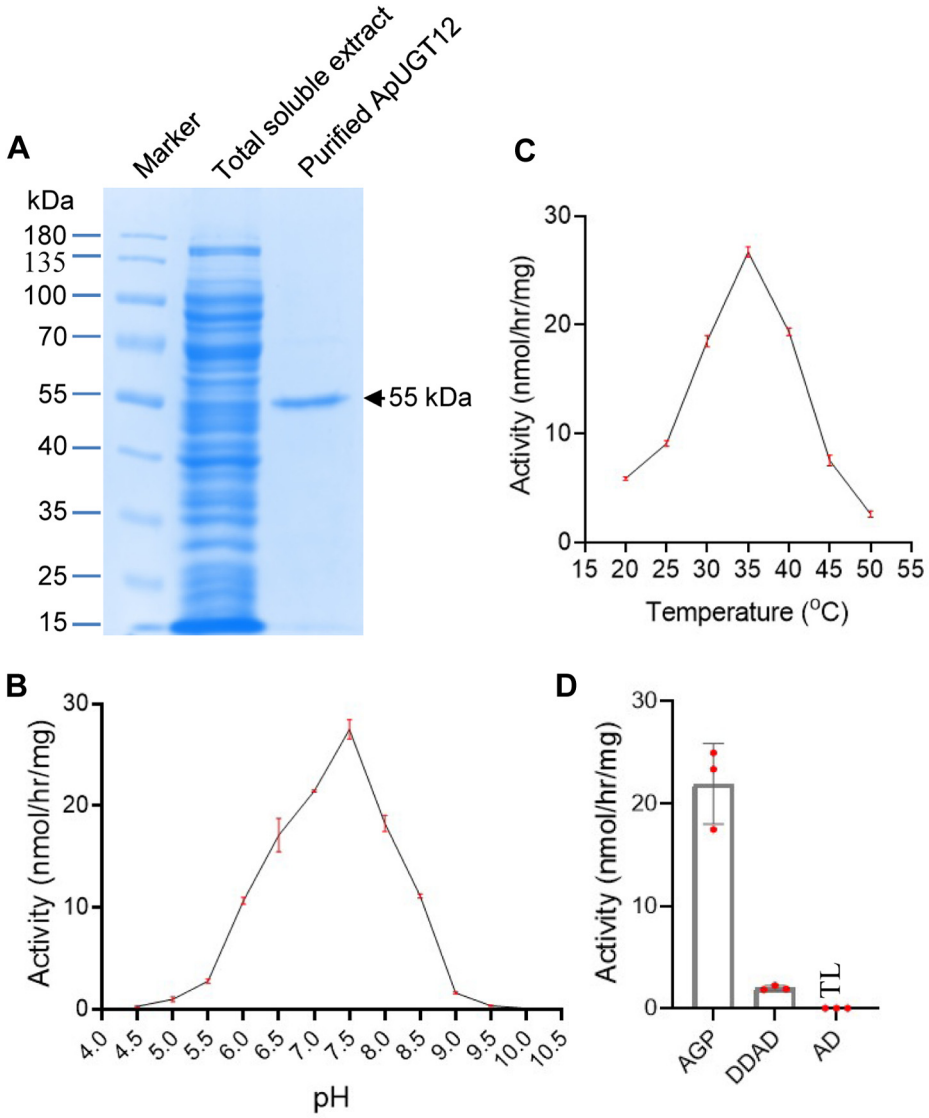

Figure 3. Bacterial expression and characterization of ApUGT12. *A*, *Escherichia coli* expression and purification of N-terminally 6×His-tagged ApUGT12. ApUGT12 was resolved as ~55 kDa protein in 10% SDS-PAGE. *B*, the optimum pH for ApUGT12 activity was determined in assays conducted at 35 °C in assay buffer of different pH. *C*, the optimum temperature for ApUGT12 activity was determined in assays in 10 mM Tris–Cl and pH 7.5 at different temperatures. *D*, a comparison of the rate of C19-O-glucosylation catalyzed by ApUGT12 using andrograpanin (AGP), andrographolide (AD), or 14-deoxy-11,12-didehydroandrographolide (DDAD). The assays were carried out in 10 mM Tris–Cl, pH 7.5 at 35 °C. *B*, *C*, and *D*, the data are means ± SD, n = 3 independent reactions using total protein extract. TL, trace level.

To understand the catalytic property of ApUGT12, steady-state kinetic parameters of recombinant ApUGT12 were determined using andrograpanin, 14-deoxy-11,12-didehydroandrographolide, and UDP-glucose. As ApUGT12 showed only trivial activity using andrographolide, the kinetic parameters could not be determined accurately using andrographolide. ApUGT12 displayed quite a dissimilar affinity for andrograpanin (K_m = 137.3 μM), 14-deoxy-11,12-didehydroandrographolide (K_m = 506.7 μM), and UDP-glucose (K_m = 271.16 μM). Moreover, k_{cat} value for andrograpanin (0.231 S^{-1}) was significantly higher than 14-deoxy-11,12-didehydroandrographolide (0.016 S^{-1}). Consequently, ApUGT12 exhibited about 48-fold higher catalytic efficiency (k_{cat}/K_m) using andrograpanin (1698.61 M^{-1} S^{-1}) than using 14-deoxy-11,12-didehydroandrographolide (34.70 M^{-1} S^{-1}). The estimated k_{cat} and k_{cat}/K_m values for 14-deoxy-11,12-didehydroandrographolide were also considerably lower than k_{cat} (0.167 S^{-1}) and k_{cat}/K_m (622.80 M^{-1} S^{-1}) values for UDP-glucose. To gain more insights into substrate specificity of ApUGT12, *in vitro* assays were carried out using UDP-glucose and a range of phytochemicals belonging to terpene, phenylpropanoid, and phenolic classes, such as steviol, kaempferol, gallic acid, 11-keto-β-boswellic acid, arjunic acid, oleanolic acid, maslinic acid, and corosolic acid (Fig. S13). However, ApUGT12 could not glucosylate any of these tested compounds. Overall, these results indicated strict scaffold selectivity of ApUGT12.

ApUGT12 subcellular localization and diterpene C19-O-glucosylation in planta

To investigate subcellular localization, ApUGT12 was expressed as enhanced yellow fluorescent protein (EYFP)–tagged

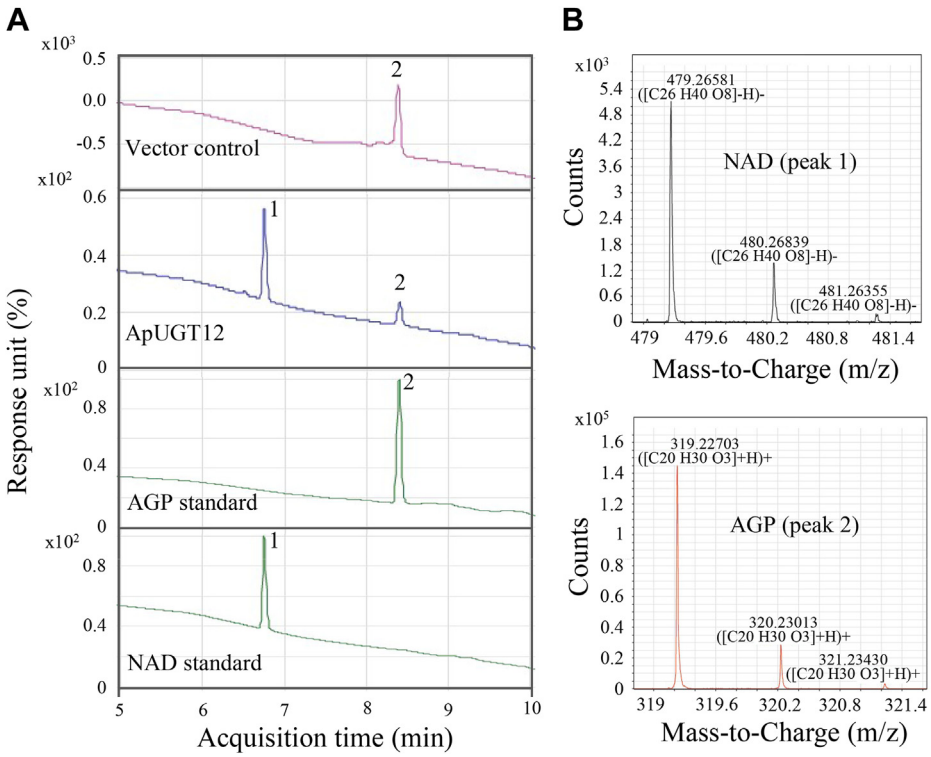

Figure 4. ApUGT12 catalyzed C19-O-glucosylation. *A*, *Escherichia coli*–expressed recombinant ApUGT12 catalyzed C19-O-glucosylation of andrograpanin (AGP) to form neoandrographolide (NAD). LC–QTOF–MS analysis identified neoandrographolide in standard and ApUGT12 assay product but not in assay conducted using total protein of *E. coli* transformed with empty vector (vector control). The assay was carried out in 10 mM Tris–Cl, pH 7.5, at 35 °C. *B*, QTOF mass spectra of neoandrographolide (peak 1) and andrograpanin (peak 2).

proteins in *Nicotiana benthamiana* leaf epidermal cells, and EYFP fluorescence in cells was examined with the help of a confocal fluorescence microscope (Fig. 5*A*). To rule out any possibility of potential subcellular localization signal at the N- or C-terminal region of ApUGT12 that might get masked because of EYFP tagging, both N- and C-terminal EYFP tagging of ApUGT12 (designated as EYFP-ApUGT12 and ApUGT12-EYFP) were carried out. P19, an RNA silencing suppressor, was also coexpressed to attain increased expression of EYFP-ApUGT12 or ApUGT12-EYFP in *N. benthamiana* leaf (49). EYFP fluorescence was detected in the cytoplasm and nucleus of cells expressing free EYFP. However, EYFP fluorescence mostly confined in the cytoplasm of cells expressing EYFP-ApUGT12 or ApUGT12-EYFP (Fig. 5*A*). To substantiate these results, EYFP-ApUGT12 or ApUGT12-EYFP was coexpressed with a cytoplasmic marker monomeric red fluorescent protein (mRFP) (50). mRFP and EYFP fluorescence were clearly merged in cells coexpressing mRFP and EYFP-ApUGT12 or ApUGT12-EYFP, confirming cytoplasmic colocalization of mRFP, EYFP-ApUGT12, and ApUGT12-EYFP proteins (Fig. 5, *B* and *C*). The cytoplasmic localization of ApUGT12 was quite reasonable because plants mostly accumulate glycosylated metabolites in vacuoles, and the transport of such metabolites is potentially driven by their glycosylation in cytoplasm (6, 11).

To know whether ApUGT12 could catalyze *in planta* diterpene C19-O-glucosylation, *N. benthamiana* leaves expressing ApUGT12-EYFP were infiltrated with andrograpanin. One-day after infiltration of andrograpanin, methanolic extracts of leaves were prepared and analyzed by HPLC. The leaves expressing ApUGT12-EYFP produced neoandrographolide when infiltrated with andrograpanin, implying that ApUGT12 catalyzed *in planta* C19-O-glucosylation of andrograpanin to produce neoandrographolide (Fig. 5*D*). However, andrograpanin infiltration in leaves expressing free EYFP (vector control) did not form neoandrographolide, suggesting that the endogenous UGT of *N. benthamiana* could not catalyze C19-O-glucosylation of andrograpanin. To substantiate these results, *in vitro* C19-O-glucosylation of andrograpanin, andrographolide, and 14-deoxy-11,12-didehydroandrographolide was tested using total protein extract of *N. benthamiana* leaves expressing *ApUGT12*. *In vitro* assays using protein extract of *ApUGT12*-expressing leaves clearly showed C19-O-glucosylation of andrograpanin to form neoandrographolide (Figs. 5*E* and S14*A*). C19-O-glucosylation of 14-deoxy-11,12-didehydroandrographolide was also achieved in assays; however, at a lower rate than andrograpanin C19-O-glucosylation (Figs. 5*E* and S14*B*). In contrast, andrographolide could not be glucosylated at a detectable level in assays using total protein extract of *ApUGT12*-expressing *N. benthamiana* leaves. Overall, these results suggest that ApUGT12 localized in the cytoplasm and catalyzed *in planta* diterpene C19-O-glucosylation.

ApUGT12 *transcript expression coincides with spatiotemporal biosynthesis of diterpene C19-O-glucoside*

To understand the involvement of ApUGT12 in spatiotemporal biosynthesis of neoandrographolide, *ApUGT12* transcript

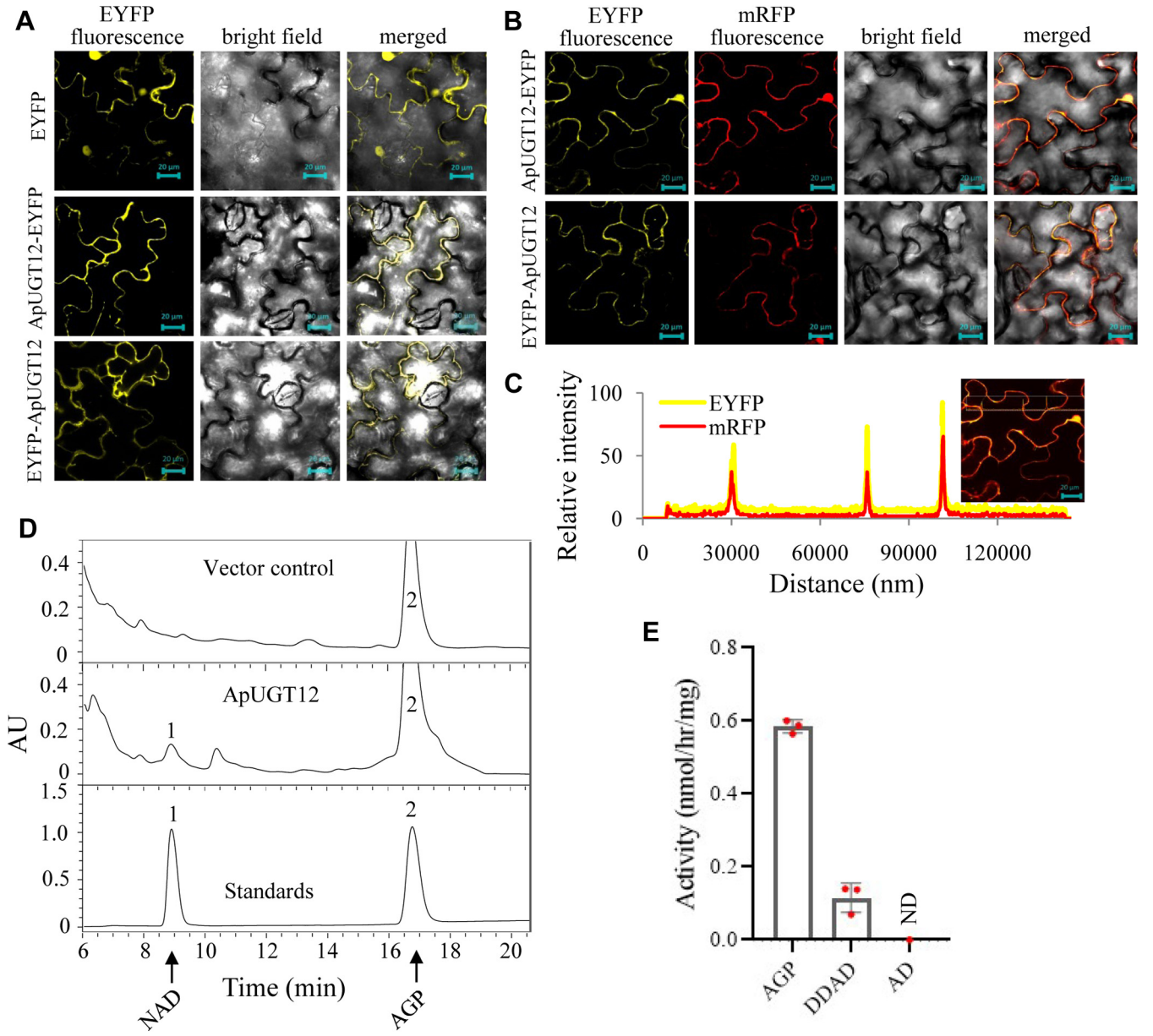

Figure 5. ApUGT12 expression in *Nicotiana benthamiana* leaf. *A*, confocal fluorescence microscopy images depicting subcellular localization of ApUGT12 in *N. benthamiana* leaf epidermal cells. C-terminal (ApUGT12-EYFP) and N-terminal (EYFP-ApUGT12) EYFP fusion constructs of ApUGT12 were transiently expressed in *N. benthamiana* leaf following agroinfiltration method. *N. benthamiana* leaf expressing EYFP served as control. The experiment was repeated three times with similar results. The scale bars represent 20 μm. *B*, the merged images showing colocalization of ApUGT12-EYFP and EYFP-ApUGT12 with the cytoplasmic marker mRFP. Scale bars, 20 μm. (C) The relative fluorescence intensity of EYFP (ApUGT12-EYFP) and mRFP was overlapped, showing colocalization of ApUGT12-EYFP and mRFP in the cytoplasm. The merged image in Figure 5*B* (*upper panel*) was reanalyzed to depict the overlapping EYFP and mRFP fluorescence along the axis marked in the inset image. The scale bar represents 20 μm. *D*, ApUGT12 catalyzed *in planta* C19-O-glucosylation of andrograpanin (AGP) to form neoandrographolide (NAD) in *N. benthamiana*. HPLC chromatograms detecting neoandrographolide (peak 1) in standard and methanolic extract of *N. benthamiana* leaves coexpressing ApUGT12-EYFP and P19. Six days post agroinfiltration, ApUGT12-EYFP–expressing leaves were infiltrated with AGP. The leaves transformed with empty vector and P19 served as vector control. The experiment was repeated three times with similar results. *E*, the relative activity of *N. benthamiana* expressed ApUGT12 using various substrates. *In vitro* assays were performed using 100 μM andrograpanin (AGP), andrographolide (AD), or 14-deoxy-11,12-didehydroandrographolide (DDAD), 800 μM UDP-glucose, and total protein extract of *N. benthamiana* leaf expressing ApUGT12-EYFP. Data are means ± SD, n = 3 independent reactions. EYFP, enhanced yellow fluorescent protein. mRFP, monomeric red fluorescent protein.

expression in kalmegh tissues was determined by qRT-PCR analysis. In accordance with increased UGT activity and neoandrographolide content, *ApUGT12* transcript expressed at an increased level in leaves of 60-day-old and 30-day-old plants (Figs. 2, *A* and *B* and 6*A*). Besides, *ApUGT12* transcript expressed at a decreased level in tissues showing reduced UGT activity and neoandrographolide content, such as in germinating seeds, roots, and petals. Moreover, MeJA-inducible expression of *ApUGT12* transcript and increased UGT activity and neoandrographolide content in leaves of MeJA-treated plants signify a potential role of ApUGT12 in MeJA-induced biosynthesis of neoandrographolide (Figs. 6*B* and S15, *A* and *B*). Taken together, the patterns of

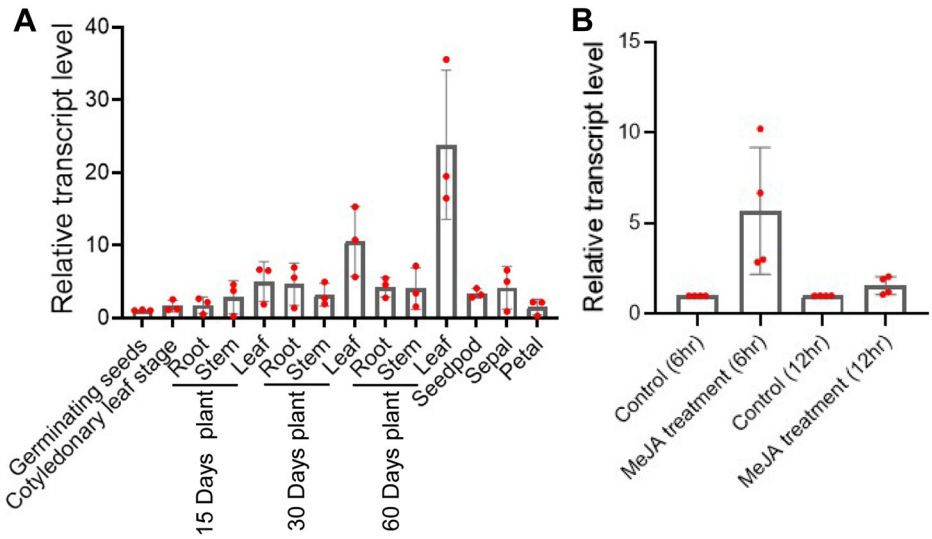

Figure 6. Spatiotemporal expression of *ApUGT12* transcript. *A*, *ApUGT12* transcript level in various tissues was determined by quantitative RT-PCR analysis. The data are means ± SD of three biological replicates. *B*, *ApUGT12* transcript level in leaves of MeJA-treated plants was determined by qRT-PCR analysis. The data are means ± SD of four biological replicates.

ApUGT12 transcript expression, UGT activity, and neoandrographolide accumulation in various tissues suggest the involvement of ApUGT12 in spatiotemporal biosynthesis of neoandrographolide.

Virus-induced gene silencing of ApUGT12

To clarify the role of ApUGT12 *in planta* biosynthesis of neoandrographolide, virus-induced gene silencing (VIGS) was carried out based on agroinfiltration method using tobacco rattle virus (TRV)–based vectors (51–53). The successful expression of TRV RNAs in agroinfiltrated seedlings was confirmed by RT-PCR detection of replicase (RdRp) and coat protein transcripts (Fig. S16). First, to confirm the effectiveness of VIGS, *ApPDS* silencing was carried out, developing the characteristic leaf photobleaching phenotype in VIGS seedlings (Fig. 7*A*) (53). The decreased expression of *ApPDS* transcript in leaves of VIGS seedlings further confirmed *ApPDS* silencing (Fig. 7*B*). Similarly, VIGS led to significant reduction (∼60%) in *ApUGT12* transcript level in leaves (Fig. 7*C*). HPLC analysis of leaf metabolites in *ApUGT12*-silenced seedlings revealed ∼50% reduction in neoandrographolide content, suggesting an essential role of ApUGT12 in the biosynthesis of major diterpene C19-O-glucoside (Fig. 7, *D* and *E*). Interestingly, andrograpanin content in *ApUGT12*-silenced seedlings was increased significantly as compared with the vector control (Fig. 7, *D* and *E*). The increased accumulation of andrograpanin in VIGS seedlings could be due to decreased rate of C19-O-glucosylation of andrograpanin to neoandrographolide because of *ApUGT12* silencing. Furthermore, to examine whether reduced content of neoandrographolide in VIGS seedlings was solely because of *ApUGT12* silencing, *UGT73AU1* and *UGT5* transcript levels were analyzed in *ApUGT12*-silenced seedlings (Fig. S17). However, unaltered transcript levels of *UGT73AU1* and *UGT5* in VIGS seedlings indicated that targeted silencing of *ApUGT12* led to a reduction in neoandrographolide content in VIGS seedlings. Overall, these results suggest a major role of ApUGT12 *in planta* biosynthesis of neoandrographolide.

ApUGT12 is a member of the poorly characterized UGT86 family

UGTs are classified into different families and subfamilies considering about 45% and 60% sequence identities, respectively. Accordingly, the UGTs of Arabidopsis and rice were grouped into different UGT families/subfamilies such as UGT71-94, UGT96-99, and UGT701–UGT710 (https://prime.vetmed.wsu.edu/resources/udp-glucuronsyltransferase-homepage). To understand phylogenetic relationship of ApUGT12 with the classified UGTs, a phylogenetic analysis was conducted based on neighbor-joining method using Arabidopsis and rice UGTs (54). In the phylogenetic tree, ApUGT12 was grouped with the Arabidopsis and rice UGT86 family members (UGT86B1, UGT86A1, and UGT86A2) to which ApUGT12 showed 41 to 46% sequence identities (Fig. 8*A*). Accordingly, the UGT committee has assigned UGT86C11 nomenclature to ApUGT12. The biochemical function of Arabidopsis and rice UGT86 family members still remains unknown. So far, a single plant UGT86 family member (UGT86C10), having about 55% sequence identity with ApUGT12, has been biochemically characterized. UGT86C10 catalyzed glucosylation of C13-apocarotenoids in *Mentha* × *piperita* (55). In contrast, ApUGT12 showed only 23 to 31% sequence identity with UGT73AU1 and UGT5 (UGT74 member), which also catalyzed andrograpanin C19-O-glucosylation (42, 43). A comparison of amino acid sequences of ApUGT12, UGT73AU1, and UGT5 identified several conserved residues, besides the UDP-sugar binding plant secondary product glycosyltransferase motif and the catalytic histidine and aspartate residues, which might determine their substrate specificity (Fig. 8*B*) (56). Overall, the identification of ApUGT12 not only helped us to understand biosynthesis of medicinal diterpene glucosides in plant but

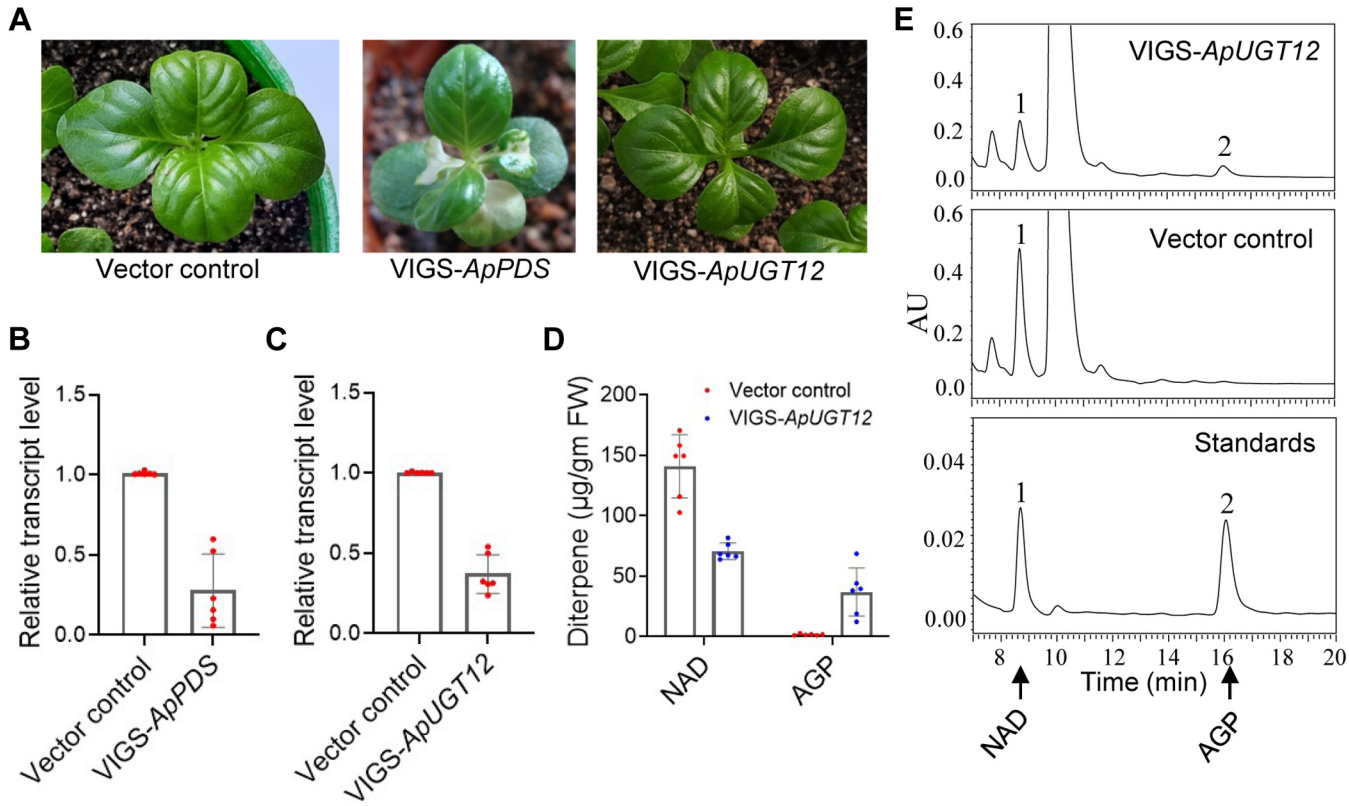

Figure 7. Virus-induced gene silencing of *ApUGT12*. *A*, Kalmegh seedlings at 35 days after vacuum infiltration with a mixture of *Agrobacterium* suspension containing pTRV1 and pTRV2-*ApPDS*/pTRV2-*ApUGT12* in a 1:1 ratio. *ApPDS* silencing led to a typical leaf photobleaching effect. Vector control represents kalmegh seedlings infiltrated with *Agrobacterium* suspension containing pTRV1 and pTRV2 empty vectors. *B*, the relative transcript level of *ApPDS* in vector control and VIGS-*ApPDS* seedlings was determined by quantitative RT-PCR. *C*, the relative transcript level of *ApUGT12* in vector control and VIGS-*ApUGT12* seedlings was determined by qRT-PCR. *D*, neoandrographolide (NAD) and andrograpanin (AGP) content in vector control and VIGS-*ApUGT12* seedlings was determined by HPLC analysis. *B–D*, the data are means ± SD, n = 6 biological samples each comprising of six seedlings. *E*, the representative HPLC chromatograms detecting neoandrographolide (NAD; peak 1) and andrograpanin (AGP; peak 2) in vector control and VIGS-*ApUGT12* samples.

also expanded our knowledge on biochemical function of a poorly characterized UGT86 family in plant specialized metabolism.

Discussion

GTs represent one of the largest enzyme families and typically account for 1 to 2% of the protein-coding genes in plants (6–8). The glycosylation of small molecules catalyzed by UGTs, the largest GT family in plants, plays crucial roles in plant development, metabolism, and stress tolerance (9, 10, 14–21, 57). In this work, we have identified a previously uncharacterized UGT86 member (ApUGT12/UGT86C11) that catalyzed C19-O-glucosylation with strict scaffold selectivity and is involved in developmental and tissue-specific biosynthesis of bioactive labdane diterpenes in the medicinal plant kalmegh. The catalytic property of recombinant ApUGT12 expressed in *E. coli* and *N. benthamiana* was very much similar to the native UGT activity detected in kalmegh (Figs. 3*D*, 5*E*, and S4). The recombinant ApUGT12 exhibited significantly higher catalytic efficiency (k_{cat}/K_m) using andrograpanin (19-hydroxy diterpene) than 14-deoxy-11,12-didehydroandrographolide (3,19-dihydroxy diterpene) (Table 1). However, ApUGT12 showed marginal activity using andrographolide (3,14,19-trihydroxy diterpene). It appears that the better catalytic efficiency of ApUGT12 using andrograpanin is likely because of the increased substrate affinity and increased rate of C19-O-glucosylation reaction. 14-Deoxy-11,12-didehydroandrographolide and andrographolide bear hydroxyl group(s) at C3 and/or C14 position, which are not found in andrograpanin (Fig. 1). Therefore, we cannot exclude the possibility that the hydroxyl group(s) at C3 and/or C14 in diterpene scaffold lead to a drastic change in rate of C19-O-glucosylation catalyzed by ApUGT12. The structure–function analysis of ApUGT12 might provide more detailed insights into scaffold-selective C19-O-glucosylation catalyzed by ApUGT12.

Two MeJA-responsive UGTs (UGT73AU1 and UGT5) were previously shown to catalyze *in vitro* C19-O-glucosylation of andrograpanin to produce neoandrographolide (42, 43). UGT73AU1 and UGT5 have marginal sequence identity (23–31%) with ApUGT12 and classified to different UGT families (UGT73 and UGT74) than ApUGT12 (UGT86). MeJA-inducible expression of *UGT73AU1* and *UGT5* transcripts could potentially contribute to MeJA-inducible neoandrographolide biosynthesis, but *UGT73AU1* and *UGT5* transcript expression patterns did not show obvious correlation with the developmental and tissue-specific biosynthesis of neoandrographolide (Figs. 2, *A* and *B*, S6, *A* and *B*, and S15, *A* and *B*). In contrast, *ApUGT12* transcript expression was not only inducible by MeJA treatment but also showed a clear

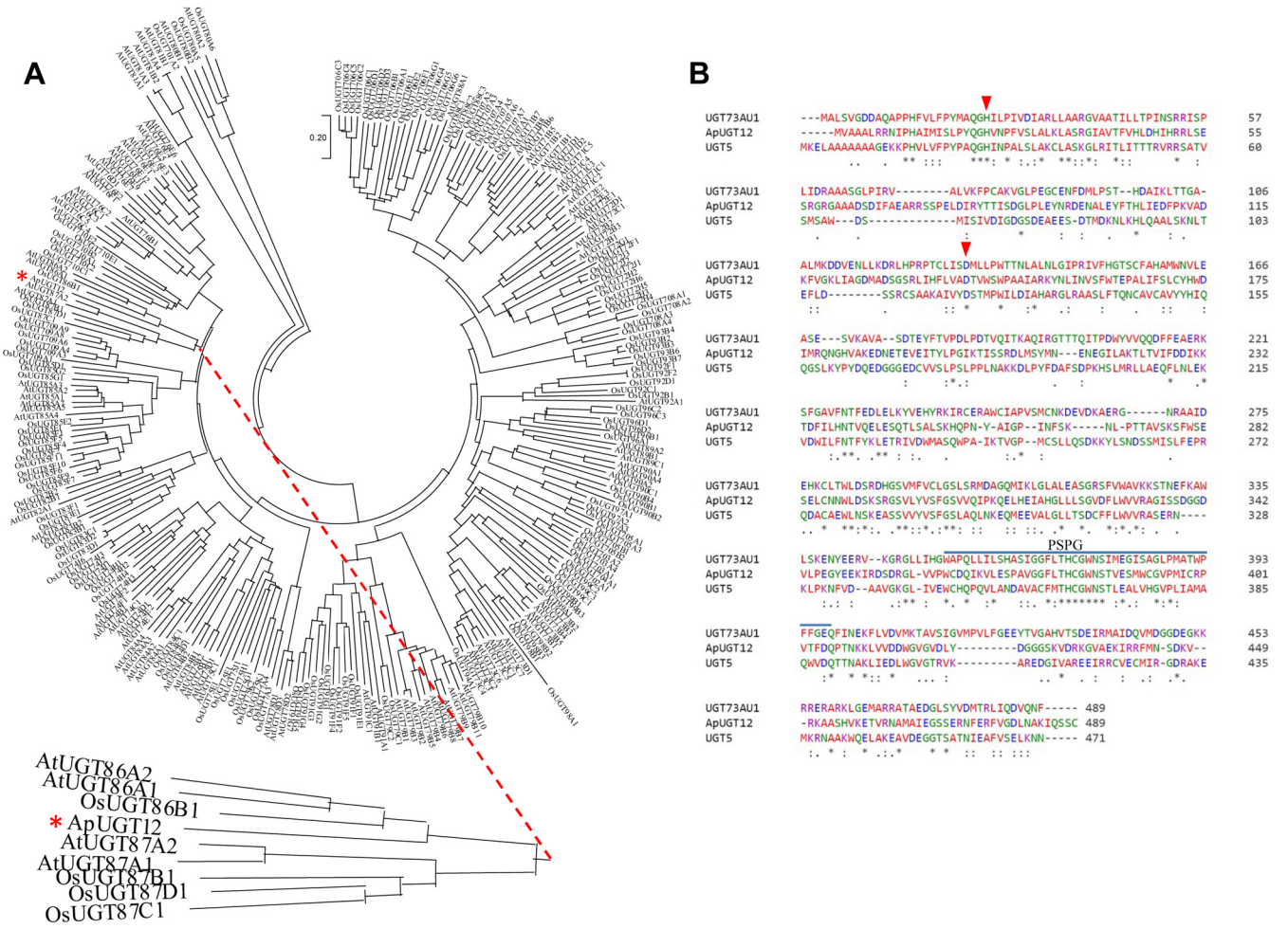

Figure 8. Phylogenetic analysis and sequence comparison of ApUGT12 with plant UGTs. *A*, the phylogenetic tree showing relationship of ApUGT12 with rice and Arabidopsis UGTs. The complete amino acid sequences of 275 UGTs obtained from the GenBank/The Arabidopsis Information Resource databases were analyzed by MEGA X software. The sequences were aligned by ClustalW, and the phylogenetic tree was constructed following the neighbor-joining method. The poisson correction method was considered for computing evolutionary distances, which are presented in the units of the number of amino acid substitutions per site. *B*, the amino acid sequence comparison of ApUGT12, UGT73AU1, and UGT5. The identical amino acid residues are depicted as asterisk (*), whereas conserved and semiconserved substitutions are marked as (:) and (.), respectively. The catalytic histidine and aspartate residues, and PSPG motif, which are conserved in UGTs, are marked with *arrowheads* and *line*. PSPG, plant secondary product glycosyltransferase; UGT, UDP-glycosyltransferase.

correlation with the developmental and tissue-specific patterns of UGT activity and neoandrographolide content (Figs. 2, *A* and *B*, 6, *A* and *B*, and S15, *A* and *B*). Further substantiating these observations, *ApUGT12* silencing led to altered profiles of diterpenes in kalmegh (Fig. 7, *C–E*). *ApUGT12*-silenced plants showed significantly depleted content of neoandrographolide and increased level of aglycone substrate andrograpanin, which was otherwise detected in a trace level, suggesting that andrograpanin is a native substrate of ApUGT12 and that *in planta* function of ApUGT12 cannot be compensated by the endogenous UGT73AU1 and UGT5 (Figs. 2*A*, 7, *C–E*, and S17). Moreover, the kinetic constants of recombinant ApUGT12 using various diterpene aglycones and the profiles of diterpene aglycones and C19-O-glucosides in *ApUGT12*-expressing tissues also suggested that andrograpanin is a preferred substrate of ApUGT12 *in planta* (Table 1 and Figs. 2*A*, 6*A*, and S3, *A* and *B*). Interestingly, andrograpanin showed promising bioactivities such as anti-inflammatory and antimicrobial properties, but, the development of andrograpanin-based products is so far compromised

Table 1
Kinetic parameters of recombinant ApUGT12

Substrate/sugar donor	K_m (μM)	V_{max} (μmolmin^{-1} mg^{-1})	k_{cat} (S^{-1})	k_{cat}/K_m (M^{-1} S^{-1})
Andrograpanin	137.3 ± 15.58	0.239 ± 0.007	0.231 ± 0.007	1698.61 ± 153.91
14-Deoxy-11,12-didehydroandrographolide	506.7 ± 197.94	0.017 ± 0.003	0.016 ± 0.003	34.70 ± 6.39
UDP-glucose	271.16 ± 36.59	0.173 ± 0.006	0.167 ± 0.005	622.80 ± 66.39

Bacterially expressed N-terminally 6×His-tagged ApUGT12 was purified and used for *in vitro* assay with sugar donor UDP-glucose and sugar acceptors (andrograpanin and 14-deoxy-11,12-didehydroandrographolide) as described in the *Experimental procedures* section. The data are the mean ± SD of three independent assays.

because of its unavailability in a sufficient quantity from kalmegh (58, 59). Hence, *ApUGT12* silencing could be a useful approach to improve andrograpanin content in plants. Overall, these results indicated a major role of ApUGT12 in developmental and tissue-specific biosynthesis of major diterpene C19-O-glucoside, whereas multiple UGTs (ApUGT12, UGT73AU1, and UGT5) might contribute to MeJA-inducible biosynthesis of diterpene C19-O-glucoside in kalmegh. Similar to *ApUGT12*, *ApCPS2* transcript also showed a clear correlation with tissue-specific biosynthesis of neoandrographolide (40). ApCPS2 having chloroplast targeting peptide potentially operates in the chloroplast; however, ApUGT12 appears to function in the cytoplasm (Fig. 5, *A*–*C*). Therefore, the diterpene biosynthetic pathway of kalmegh potentially represents an example of specialized metabolic pathways, which are compartmentalized in multiple subcellular organelles and predominantly under the transcriptional regulation (2).

Labdane diterpenes with about 7000 known structures are a large family of natural products (27). The terpene synthases catalyzing the early steps in labdane diterpene biosynthesis were very well characterized, but the enzymes involved in the late-stage structural modifications such as those catalyzing regioselective glycosylation were not well studied (60–63). Previously, UGT73 to UGT76 and UGT85 members were shown to catalyze labdane diterpene glycosylation in plants, but the role of UGT86 in diterpene glycosylation was not known before (17, 42, 43, 64). ApUGT12 is a new addition to the list of UGT families participating in diterpene glycosylation. Indeed, UGT86 represents one of the poorly studied UGT families in plants (7, 13). Until now, a single member of the UGT86 family (UGT86C10) was biochemically characterized (55). UGT86C10 catalyzing glucosylation of C13-apocarotenoids has quite a dissimilar substrate selectivity than ApUGT12, suggesting that UGT86 potentially plays diverse roles in plant specialized metabolism. It appears that ApUGT12 is very specific to the kalmegh labdane diterpene pathway and has rigid substrate selectivity because it could not glycosylate a range of other tested phytochemicals belonging to the terpene, phenylpropanoid, and phenolic classes, including steviol, another labdane diterpene (Fig. S13). Unlike Arabidopsis and rice that encode only one to two UGT86 members, it appears that UGT86 family expanded remarkably in kalmegh, resulting in at least six UGT86 members (UGT86C7, UGT86C11, UGT86C12, UGT86E1, UGT86L1, and UGT86K1), which showed leaf-preferential transcript expression. Furthermore, studies on UGT86 family members in diverse plants could provide a more detail information on the diversity of function they might play in plants. In conclusion, the discovery of ApUGT12 not only advanced our understanding of the biochemical function of UGTs in plant specialized metabolism but also opened up the prospect for genetic improvement of plants toward a specific diterpene chemotype.

Experimental procedures

Plant materials

Kalmegh plants (Cv. CIM-Megha) were grown in earthen pots under the natural light during the months of July to October, and samples were collected during different plant growth stages as described previously (40). MeJA (250 μM) treatment was given to 30-day-old plants as described previously (65). *N. benthamiana* was grown in Conviron A1000 plant growth chamber as described previously (66). Plant samples were flash frozen in liquid nitrogen and preserved at −80 °C until further use for isolation of proteins, metabolites, and RNA.

RNA extraction and qRT-PCR analysis

RNA isolation was done as described previously (67). RNA was cleaned up using RNeasy kit (Qiagen), DNaseI-treated, and processed for cDNA preparation using MultiScribe reverse transcriptase (Thermo Fisher Scientific). qRT-PCR was carried out in 7900HT Fast Real Time PCR using Power SYBR Green Master Mix (Thermo Fisher Scientific) with at least two technical replicates per cDNA sample. The amplification specificity was examined by analyzing melting curves at the dissociation step. The relative transcript expression was analyzed by following the $2^{-\Delta\Delta ct}$ method. *ApRSP4* and *ApEF1-α* were selected as the reference genes for normalization of qRT-PCR data based on an analysis of expression stability of the selected traditional reference genes including *ApTUB*, *ApActin*, *ApPP2A*, *ApUBC*, *ApRSP4*, and *ApEF1-α* (Fig. S18). Oligonucleotide sequences used in qRT-PCR analysis are listed in Table S2.

Bacterial expression and purification of recombinant protein

ApUGT coding sequences were PCR amplified from leaf cDNAs using Phusion high-fidelity DNA polymerase (Thermo Fisher Scientific) and gene-specific oligonucleotides (Table S2) and cloned into pET-28a(+). The integrity of the plasmid constructs was confirmed through sequencing using Big Dye terminator kit (Thermo Fisher Scientific). The confirmed plasmids were individually transformed into *E. coli* strain BL21 codon plus (DE3) RIPL. The transformants were precultured for overnight at 37 °C in LB media (5 ml) containing kanamycin (50 μg/ml), chloramphenicol (35 μg/ml), and streptomycin (100 μg/ml). The secondary culture was initiated using 0.01% of overnight grown primary culture and allowed to grow until an absorbance to 0.8 was reached at 600 nm. The culture was then incubated at 16 °C for 30 min, and after addition of 0.5 mM IPTG, it was further grown at 16 °C for overnight. Bacterial cells were harvested by centrifugation (2500*g* for 15 min) and washed with lysis buffer (50 mM Tris–Cl, pH 7.5, 150 mM NaCl, 10 mM $MgCl_2$, and 10% glycerol). The cell pellet was resuspended in ice-cold lysis buffer supplemented with 10 mM imidazole, 1% Tween-20, 5 mM DTT, 0.1 mM PMSF, 1× EDTA-free protease inhibitor cocktail (Sigma–Aldrich), 0.5 mg/ml lysozyme, 2.5 units/ml benzonase (Merck Millipore), and incubated in ice for 30 min. Cell lysate was prepared by sonication for six to eight cycles (30 s ON and 99 s OFF at 50% amplitude). The soluble protein fraction was obtained after centrifugation (18,000*g* at 4 °C for 30 min) and subjected to affinity chromatography using Ni–NTA agarose (Qiagen). To prepare enriched fraction of recombinant UGT

for use in initial screening of UGT activity, the soluble protein of 100 ml bacterial culture was bound to pre-equilibrated Ni–NTA agarose (100 μl) for 2 to 3 h at 4 °C, passed through a 10 ml gravity column (Bio-Rad), washed with lysis buffer containing 20 mM imidazole, and eluted with lysis buffer containing 250 mM imidazole (68). For purification of ApUGT12 to electrophoretic homogeneity, soluble protein of 1 l bacterial culture was bound to pre-equilibrated Ni–NTA agarose (1 ml), passed through a 1 ml chromatography column (Bio-Rad) equipped with a peristaltic pump (Miclins India) and a fraction collector (Bio-Rad). The bound protein was washed in a step-wise gradient manner using lysis buffer containing 50 to 100 mM imidazole and eluted with lysis buffer containing 250 mM imidazole. The fractions of recombinant protein were pooled, desalted (50 mM Tris–Cl, pH 7.5, 150 mM NaCl, 10% glycerol, and 1 mM DTT), and concentrated using a 10 kDa cutoff centrifugal filter (Merck Millipore). The purity of protein was analyzed in SDS-PAGE with Coomassie blue stain, and protein concentration was determined following the Bradford method using bovine serum albumin (BSA) standard (69) and also by measuring UV absorption at an absorbance at 280 nm (Nanodrop spectrophotometer). The quantity of purified protein was also verified by densitometric analysis of SDS-PAGE gel with known quantity of BSA using ImageJ software (National Institutes of Health).

Transient expression in N. benthamiana

ApUGT12 was cloned into pGWB441 and pGWB442 for N- and C-terminal EYFP tagging. ApUGT12 was amplified using Phusion high-fidelity DNA polymerase with ORF-specific primers (Table S2), inserted into pENTR D-TOPO (Invitrogen), and finally cloned into pGWB441 and pGWB442 following LR clonase reaction (70). Empty pGWB441 and pGWB454 for expressing free EYFP and mRFP were prepared by recombining empty pENTR/D-TOPO plasmid with pGWB441 and pGWB454 (68). The recombinant clones were selected in LB media containing spectinomycin (100 μg/ml). The clones were confirmed by sequencing and transformed into *Agrobacterium tumefaciens* (EHA105) following freeze-thaw method (71). For transient expression of recombinant proteins in *N. benthamiana* leaf, *Agrobacterium* suspension was prepared in infiltration buffer (10 mM MES, pH 5.6, 10 mM $MgCl_2$, and 200 μM acetosyringone), and agroinfiltration method was followed as described previously using 5- to 6-week-old plants (66). P19, a post-transcriptional gene silencing suppressor, was coexpressed from pBin61-P19 plasmids along with recombinant ApUGT12 (49). After 36 to 48 h of agroinfiltration, leaf sections were analyzed, and images were captured under a Carl Zeiss LSM880 laser scanning confocal microscope using 63× (numerical aperture of 1.4) oil-immersion objective. YFP was excited at 514 nm and detected in a range of 525 to 562 nm, whereas RFP was excited at 561 nm and detected in a range of 570 to 652 nm (68). The simultaneous detection of RFP and YFP was done by combining the settings mentioned previously in the sequential scanning function of the microscope as per manufacturer's instructions. Six days after agroinfiltration, leaves were infiltrated with andrograpanin for *in planta* UGT assay or processed for protein isolation.

VIGS

ApUGT12 cDNA fragments from the 3′ end (472 bp) and 5′ end (419 bp) were PCR amplified using gene-specific primers and inserted in pTRV2 vector (Table S2). pTRV2-*ApPDS* constructs for VIGS were described previously (53). pTRV2 constructs were individually transformed into *A. tumefaciens* (GV3101). VIGS was performed in kalmegh seedlings at cotyledonary leaf stage (7–10 days old) as described previously with few modifications (53). *Agrobacterium* carrying pTRV1 and pTRV2 plasmids were cultured in 50 ml LB containing 10 mM MES, 20 μM acetosyringone, 50 μg/ml kanamycin, and 25 μg/ml rifampicin until an absorbance at 600 nm reached to 1.8 to 2.0. Subsequently, *Agrobacterium* were resuspended in infiltration buffer (10 mM MES, pH 5.6, 200 μM acetosyringone, and 10 mM $MgCl_2$) to achieve a final absorbance of 1.0 at 600 nm and incubated at room temperature for 2 to 4 h. Before agroinfiltration, *Agrobacterium* containing pTRV1 and pTRV2 plasmids were mixed in equal ratio. For the silencing of *ApPDS* and *ApUGT12*, *Agrobacterium* harboring pTRV2 construct targeting 3′ or 5′ region of *ApPDS/ApUGT12* cDNAs were mixed in equal ratio before adding (equal proportion) to *Agrobacterium* carrying pTRV1. Vacuum infiltration of *Agrobacterium* into kalmegh seedlings was done as described previously (53). After agroinfiltration, excess liquid from seedlings was soaked in blotting paper, and seedlings were planted into soilrite mix, covered with polyethylene bags, and maintained in dark for 12 to 24 h. Seedlings were subsequently grown at 24 to 25 °C temperature with a 16:8 h light:dark cycle in a glass house. The seedlings at 30 to 35 days of agroinfiltration frequently showed *ApPDS*-silencing phenotype in leaves, but the new leaves emerged thereafter did not always have silencing phenotype (53). Therefore, the leaves were harvested after 30 to 35 days of agroinfiltration, flash frozen in liquid nitrogen, and stored at −80 °C until further use.

UGT assay

To isolate proteins from kalmegh tissues and *ApUGT12*-transformed *N. benthamiana* leaves for *in vitro* UGT assays, frozen samples (1 g) were ground to fine powder in liquid nitrogen using mortar and pestle, and protein was extracted in 5 ml precooled buffer (100 mM Tris–Cl, pH 7.5, 5 mM DTT, 150 mM NaCl, 5% glycerol, 0.1 mM PMSF, and 1× protease inhibitor cocktail) at 4 °C for 2 h. Soluble protein fraction was collected by centrifugation (18,000*g* at 4 °C for 30 min) and quantified in Bradford assays using BSA standard. Until otherwise mentioned, *in vitro* UGT assay was carried out in 50 μl assay buffer (10 mM Tris–Cl, pH 7.5, and 1 mM DTT) containing 250 μM sugar acceptor (andrograpanin, andrographolide, 14-deoxy-11,12-didehydroandrographolide, or other phytochemicals), 2 mM UDP-glucose, and 30 to 50 μg of total protein extract or 2.5 μg of

purified protein, at 35 °C for 15 to 60 min with continuous shaking at 200 rpm. The reaction was stopped by adding 200 µl ethyl acetate, the organic phase was collected by centrifugation (15,000*g* for 5 min), air dried, and finally dissolved in methanol for TLC analysis using chloroform:toluene:methanol (66:26:8) solvent mixture as a mobile phase (40) or processed for HPLC and LC–QTOF–MS analysis as described later. To determine optimum pH for ApUGT12 activity, reactions were set in 100 mM sodium acetate (pH 4.5–5.0), 100 mM MES–HCl (pH 5.5–6.5), 100 mM Tris–Cl (pH 7.0–8.5), or 100 mM sodium carbonate–bicarbonate buffer (pH 9.0–10.0). To know optimum temperature for ApUGT12 activity, the assays were performed at temperatures ranging from 20 to 50 °C in assay buffer. For determining the kinetic parameters, *in vitro* assays were done using 15 to 1500 µM andrograpanin or 14-deoxy-11,12-didehydroandrographolide, 2.5 mM UDP-glucose, and 2.5 µg purified ApUGT12 in 50 µl assay buffer at 35 °C for 15 min. The kinetic constants for UDP-glucose were determined in assays containing 30 to 2500 µM UDP-glucose and 500 µM andrograpanin. The product formed in the assays was estimated with a comparison to standard curve by HPLC analysis, and kinetic parameters (V_{max}, K_m, and k_{cat}) were determined by nonlinear regression analysis and fitting into Michaelis–Menten model using GraphPad Prism 9.1.2 (GraphPad Software, Inc) for Windows (www.graphpad.com). Because of unavailability of pure 14-deoxy-11,12-didehydroandrographiside standard, the rate of reaction using 14-deoxy-11,12-didehydroandrographolide was calculated based on the amount of substrate consumed in reactions. ApUGT12 activity toward varied phytochemicals (steviol, kaempferol, gallic acid, oleanolic acid, corosolic acid, maslinic acid, arjunic acid, and 11-keto-β-boswellic acid) was analyzed in assay buffer as described previously. *In planta*, ApUGT12 activity in *N. benthamiana* leaves was also done as described previously with few modifications (72). Six days after agroinfiltration, *N. benthamiana* leaf discs (2 cm diameter) were prepared and dipped in infiltration buffer containing 250 µM andrograpanin, and vacuum was applied (600 mm Hg for 3 min). Subsequently, leaf discs were placed on wet blotting paper in Petri dish and kept in plant growth chamber. After 24 h of incubation, leaf discs were washed thoroughly in pure water, flash frozen in liquid nitrogen, lyophilized, and stored at −80 °C until further use.

Metabolite extraction and HPLC analysis

Flash-frozen plant samples were ground to fine powder in liquid nitrogen using pestle and mortar. The ground tissue (250 mg) was extracted twice with 5 ml methanol. The organic phase was collected by centrifugation (18,000*g* for 15 min), evaporated to dryness, and finally reconstituted in methanol. Lyophilized leaf discs were ground to fine powder in liquid nitrogen, and ground tissue (100 mg) was extracted with 5 ml methanol. HPLC separation of plant metabolites and UGT assay products was carried out in an isocratic elution mode using a Waters Spherisorb ODS2 column (250 × 4.6 mm, 5 µm particle size) and a Waters Alliance e2695 separation module HPLC system consisting of a 2998 photodiode array detector, autosampler, vacuum degasser, and quaternary pump (Waters) as described previously (73). The mobile phase consisted of a mixture of solvents: acetonitrile (solvent A: 15%) and 60:40 methanol–water (solvent B: 85%) with 0.6 ml/min constant flow rate and 25 °C column temperature. The stock solutions (1 mg/ml) of andrographolide, andrographiside, andrograpanin, neoandrographolide, and 14-deoxy-11,12-didehydroandrographolide (Sigma–Aldrich and Natural Remedies) were made in methanol for standard curve preparation. Metabolite peaks were monitored at 200 to 220 nm considering retention time and UV spectra, and quantification was performed with a comparison to the standard curve. Steviol, kaempferol, gallic acid, arjunic acid, oleanolic acid, corosolic acid, maslinic acid, and 11-keto-β-boswellic acid were analyzed as per HPLC methods described previously (74–76).

LC–QTOF–MS analysis

The Agilent 1290 Infinity II UPLC system coupled with an Agilent 6545A QTOF mass spectrometer was used for LC–QTOF–MS analysis. The UPLC system consisted of a solvent reservoir, a degasser, a G7120A binary pump, a G7130A column oven, a G7129B vial sampler, and a G4212B diode array detector. The mass spectrometer was based on an Agilent multimode ion source. The liquid chromatographic separation was performed considering gradient elution on a Zorbax Eclipse Plus C18 Rapid Resolution HD (2.1 × 50 mm, 1.8 µm) column with a set flow rate at 0.2 ml/min and temperature at 30 °C (77). The mobile phase consisted of 0.1% formic acid aqueous solution (solution A) and acetonitrile (solution B), and the gradient elution was carried out as follows: 0 to 3 min, 20% B; 3 to 4.5 min, 30% B; 4.5 to 6 min, 50% B; 6 to 8.5 min, 70% B; 8.5 to 10 min, 90% B; 10 to 12 min, 50% B; and 12 to 15 min, 10% B. Before sample analysis, the column was saturated using the mobile phase for at least 30 min. Diode array detector spectrum was recorded in the wavelength range from 190 to 600 nm with a peak width >0.1 min (2 s response time) at 2.5 Hz. The QTOF–MS was run in both positive and negative modes. The chromatographic and spectra data (.d) were obtained using Agilent Mass Hunter Data Acquisition software (version B.06.01). The operation conditions of the mass spectrometer were as follows: drying gas (nitrogen) temperature, 325 °C; drying gas flow rate, 10 l/min; nebulizer gas (nitrogen) pressure, 35 psi; capillary voltage, 2500 V; fragmentor voltage, 180 V; skimmer voltage, 45 V; and octupole radiofrequency voltage, 750 V. The data were acquired by MS1 mode. The MS scan range was 100 to 1700 m/z at a scan rate of 1.5 spectra/s. The mass spectrometer was calibrated and tuned before analysis for accuracy in the mass.

Data availability

The sequence data are deposited in the GenBank with accession numbers MW589262-MW589284 (ApUGT1-ApUGT23) and KU516822 (ApPDS).

Supporting information—This article contains supporting information (41).

Acknowledgments—The authors gratefully acknowledge the Biological and Chemical Central Facility and the Director, Council of

Scientific and Industrial Research-Central Institute of Medicinal and Aromatic Plants for research facilities; Prof Sir David Baulcombe for pBIN61-P19; Prof Tsuyoshi Nakagawa for pGWB plasmids; and Prof Michael Court for UGT nomenclature. Institutional communication number for this article is CIMAP/PUB/2021/MAR/15.

Author contributions—S. G. conceptualization; P.S. and S. G. methodology; P. S., C. S. C., and S. G. formal analysis; P. S., A. G., and R. C. M. investigation; P. S. data curation; P. S. and S. G. writing–original draft; S. G. writing–review and editing; S. G. supervision.

Funding and additional information—S. G. received research grants from the Indian National Science Academy (SP/YSP/126/2016/217) and the Council of Scientific and Industrial Research (HCP-10). P. S. acknowledges the CSIR for research fellowship.

Conflict of interest—The authors declare that they have no conflicts of interest with the contents of this article.

Abbreviations—The abbreviations used are: BSA, bovine serum albumin; cDNA, complementary DNA; EYFP, enhanced yellow fluorescent protein; GT, glycosyltransferase; MeJA, methyl jasmonate; mRFP, monomeric red fluorescent protein; Ni–NTA, nickel–nitrilotriacetic acid; qRT-PCR, quantitative RT-PCR; QTOF, quadrupole TOF; TRV, tobacco rattle virus; UGT, UDP-glycosyltransferase; VIGS, virus-induced gene silencing.

References

1. Pichersky, E., and Raguso, R. A. (2018) Why do plants produce so many terpenoid compounds? *New Phytol.* **220**, 692–702
2. Lacchini, E., and Goossens, A. (2020) Combinatorial control of plant specialized metabolism: Mechanisms, functions, and consequences. *Annu. Rev. Cell. Dev. Biol.* **36**, 291–313
3. Erb, M., and Kliebenstein, D. J. (2020) Plant secondary metabolites as defenses, regulators, and primary metabolites: The blurred functional trichotomy. *Plant Physiol.* **184**, 39–52
4. Fernie, A. R., and Tohge, T. (2017) The genetics of plant metabolism. *Annu. Rev. Genet.* **51**, 287–310
5. Chae, L., Kim, T., Nilo-Poyanco, R., and Rhee, S. Y. (2014) Genomic signatures of specialized metabolism in plants. *Science* **344**, 510–513
6. Lairson, L. L., Henrissat, B., Davies, G. J., and Withers, S. G. (2008) Glycosyltransferases: Structures, functions, and mechanisms. *Annu. Rev. Biochem.* **77**, 521–555
7. Yonekura-Sakakibara, K., and Hanada, K. (2011) An evolutionary view of functional diversity in family 1 glycosyltransferases. *Plant J.* **66**, 182–193
8. Lim, E. K., and Bowles, D. J. (2004) A class of plant glycosyltransferases involved in cellular homeostasis. *EMBO J.* **23**, 2915–2922
9. Louveau, T., Orme, A., Pfalzgraf, H., Stephenson, M. J., Melton, R., Saalbach, G., Hemmings, A. M., Leveau, A., Rejzek, M., Vickerstaff, R. J., Langdon, Field, R., and Osbourn, A. (2018) Analysis of two new arabinosyltransferases belonging to the carbohydrate-active enzyme (CAZY) glycosyltransferase family 1 provides insights into disease resistance and sugar donor specificity. *Plant Cell* **30**, 3038–3057
10. Adiji, O. A., Docampo-Palacios, M. L., Alvarez-Hernandez, A., Pasinetti, G. M., Wang, X., and Dixon, R. A. (2021) UGT84F9 is the major flavonoid UDP-glucuronosyltransferase in *Medicago truncatula*. *Plant Physiol.* **185**, 1617–1637
11. Bowles, D., Lim, E. K., Poppenberger, B., and Vaistij, F. E. (2006) Glycosyltransferases of lipophilic small molecules. *Annu. Rev. Plant Biol.* **57**, 567–597
12. Tiwari, P., Sangwan, R. S., and Sangwan, N. S. (2016) Plant secondary metabolism linked glycosyltransferases: An update on expanding knowledge and scopes. *Biotechnol. Adv.* **34**, 714–739
13. Wilson, A. E., and Tian, L. (2019) Phylogenomic analysis of UDP-dependent glycosyltransferases provides insights into the evolutionary landscape of glycosylation in plant metabolism. *Plant J.* **100**, 1273–1288
14. Cai, J., Jozwiak, A., Holoidovsky, L., Meijler, M. M., Meir, S., Rogachev, I., and Aharoni, A. (2021) Glycosylation of N-hydroxy-pipecolic acid equilibrates between systemic acquired resistance response and plant growth. *Mol. Plant* **14**, 440–455
15. Nagatoshi, M., Terasaka, K., Nagatsu, A., and Mizukami, H. (2011) Iridoid-specific glucosyltransferase from *Gardenia jasminoides*. *J. Biol. Chem.* **286**, 32866–32874
16. Owatworakit, A., Townsend, B., Louveau, T., Jenner, H., Rejzek, M., Hughes, R. K., Saalbach, G., Qi, X., Bakht, S., Roy, A. D., Mugford, S. T., Goss, R. J., Field, R. A., and Osbourn, A. (2013) Glycosyltransferases from oat (Avena) implicated in the acylation of avenacins. *J. Biol. Chem.* **288**, 3696–3704
17. Richman, A., Swanson, A., Humphrey, T., Chapman, R., McGarvey, B., Pocs, R., and Brandle, J. (2005) Functional genomics uncovers three glucosyltransferases involved in the synthesis of the major sweet glucosides of *Stevia rebaudiana*. *Plant J.* **41**, 56–67
18. Seki, H., Tamura, K., and Muranaka, T. (2015) P450s and UGTs: Key players in the structural diversity of triterpenoid saponins. *Plant Cell Physiol* **56**, 1463–1471
19. Wu, B., Cao, X., Liu, H., Zhu, C., Klee, H., Zhang, B., and Chen, K. (2019) UDP-glucosyltransferase PpUGT85A2 controls volatile glycosylation in peach. *J. Exp. Bot.* **70**, 925–936
20. Jing, T., Zhang, N., Gao, T., Wu, Y., Zhao, M., Jin, J., Du, W., Schwab, W., and Song, C. (2020) UGT85A53 promotes flowering via mediating abscisic acid glucosylation and FLC transcription in *Camellia sinensis*. *J. Exp. Bot.* **71**, 7018–7029
21. Li, Y. J., Wang, B., Dong, R. R., and Hou, B. K. (2015) AtUGT76C2, an Arabidopsis cytokinin glycosyltransferase is involved in drought stress adaptation. *Plant Sci.* **236**, 157–167
22. Kim, M. J., Zheng, J., Liao, M. H., and Jang, I. C. (2019) Overexpression of SrUGT76G1 in Stevia alters major steviol glycosides composition towards improved quality. *Plant Biotechnol. J.* **17**, 1037–1047
23. He, Y., Wu, L., Liu, X., Jiang, P., Yu, L., Qiu, J., Wang, G., Zhang, X., and Ma, H. (2020) TaUGT6, a novel UDP-glycosyltransferase gene enhances the resistance to FHB and DON accumulation in wheat. *Front. Plant Sci.* **11**, 574775
24. Brazier-Hicks, M., Offen, W. A., Gershater, M. C., Revett, T. J., Lim, E. K., Bowles, D. J., Davies, G. J., and Edwards, R. (2007) Characterization and engineering of the bifunctional N- and O-glucosyltransferase involved in xenobiotic metabolism in plants. *Proc. Natl. Acad. Sci. U. S. A.* **104**, 20238–20243
25. Tognetti, V. B., Van Aken, O., Morreel, K., Vandenbroucke, K., van, de, Cotte, B., De, Clercq, I., Chiwocha, S., Fenske, R.,, Prinsen, E., Boerjan, W., Genty, B., Stubbs, K. A., Inzé, D., Van, *et al.* (2010) Perturbation of indole-3-butyric acid homeostasis by the UDP-glucosyltransferase UGT74E2 modulates Arabidopsis architecture and water stress tolerance. *Plant Cell* **22**, 2660–2679
26. Haroth, S., Feussner, K., Kelly, A. A., Zienkiewicz, K., Shaikhqasem, A., Herrfurth, C., and Feussner, I. (2019) The glycosyltransferase UGT76E1 significantly contributes to 12-O-glucopyranosyl-jasmonic acid formation in wounded *Arabidopsis thaliana* leaves. *J. Biol. Chem.* **294**, 9858–9872
27. Peters, R. J. (2010) Two rings in them all: The labdane-related diterpenoids. *Nat. Prod. Rep.* **27**, 1521–1530
28. Koteswara, Rao, Y., Vimalamma, G., Rao, C. V., and Tzeng, Y. M. (2004) Flavonoids and andrographolides from *Andrographis paniculata*. *Phytochem.* **65**, 2317–2321
29. Valdiani, A., Talei, D., Lattoo, S. K., Ortiz, R., Rasmussen, S. K., Batley, J., Rafii, M. Y., Maziah, M., Sabu, K. K., Abiri, R., Sakuanrungsirikul, S., and Tan, S. G. (2017) Genoproteomics-assisted improvement of *Andrographis paniculata*: Toward a promising molecular and conventional breeding platform for autogamous plants affecting the pharmaceutical industry. *Crit. Rev. Biotechnol.* **37**, 803–816
30. Burgos, R. A., Alarcón, P., Quiroga, J., Manosalva, C., and Hancke, J. (2020) Andrographolide, an anti-inflammatory multitarget drug: All roads lead to cellular metabolism. *Molecules* **26**, 5

31. Jiang, M., Sheng, F., Zhang, Z., Ma, X., Gao, T., Fu, C., and Li, P. (2021) *Andrographis paniculata* (Burm.f.) Nees and its major constituent andrographolide as potential antiviral agents. *J. Ethnopharmacol.* **272**, 113954
32. Lo, C. W., Lii, C. K., Hong, J. J., Chuang, W. T., Yang, Y. C., Huang, C. S., and Chen, H. W. (2021) Andrographolide inhibits IL-1β release in bone marrow-derived macrophages and monocyte infiltration in mouse knee joints induced by monosodium urate. *Toxicol. Appl. Pharmacol.* **410**, 115341
33. Kapil, A., Koul, I. B., Banerjee, S. K., and Gupta, B. D. (1993) Anti-hepatotoxic effects of major diterpenoid constituents of *Andrographis paniculata*. *Biochem. Pharmacol.* **46**, 182–185
34. Wiart, C., Kumar, K., Yusof, M. Y., Hamimah, H., Fauzi, Z. M., and Sulaiman, M. (2005) Antiviral properties of ent-labdene diterpenes of *Andrographis paniculata* nees, inhibitors of herpes simplex virus type 1. *Phytother. Res.* **19**, 1069–1070
35. Liu, J., Wang, Z. T., and Ji, L. L. (2007) *In vivo* and *in vitro* anti-inflammatory activities of neoandrographolide. *Am. J. Chin. Med.* **35**, 317–328
36. Yang, T., Shi, H. X., Wang, Z. T., and Wang, C. H. (2013) Hypolipidemic effects of andrographolide and neoandrographolide in mice and rats. *Phytother. Res.* **27**, 618–623
37. Nantajit, D., Jetawattana, S., Suriyo, T., Grdina, D. J., and Satayavivad, J. (2017) *Andrographis paniculata* diterpenoids protect against radiation-induced transformation in BALB/3T3 cells. *Radiat. Res.* **188**, 66–74
38. Batkhuu, J., Hattori, K., Takano, F., Fushiya, S., Oshiman, K., and Fujimiya, Y. (2002) Suppression of NO production in activated macrophages *in vitro* and ex vivo by neoandrographolide isolated from *Andrographis paniculata*. *Biol. Pharm. Bull.* **25**, 1169–1174
39. Pfisterer, P. H., Rollinger, J. M., Schyschka, L., Rudy, A., Vollmar, A. M., and Stuppner, H. (2010) Neoandrographolide from *Andrographis paniculata* as a potential natural chemosensitizer. *Planta Med.* **76**, 1698–1700
40. Misra, R. C., Garg, A., Roy, S., Chanotiya, C. S., Vasudev, P. G., and Ghosh, S. (2015) Involvement of an ent-copalyl diphosphate synthase in tissue-specific accumulation of specialized diterpenes in *Andrographis paniculata*. *Plant Sci.* **240**, 50–64
41. Garg, A., Agrawal, L., Misra, R. C., Sharma, S., and Ghosh, S. (2015) *Andrographis paniculata* transcriptome provides molecular insights into tissue-specific accumulation of medicinal diterpenes. *BMC Genomics* **16**, 659
42. Li, Y., Lin, H. X., Wang, J., Yang, J., Lai, C. J., Wang, X., Ma, B. W., Tang, J. F., Li, Y., Li, X. L., Guo, J., Gao, W., and Huang, L. Q. (2018) Glucosyltransferase capable of catalyzing the last step in neoandrographolide biosynthesis. *Org. Lett.* **20**, 5999–6002
43. Sun, W., Leng, L., Yin, Q., Xu, M., Huang, M., Xu, Z., Zhang, Y., Yao, H., Wang, C., Xiong, C., Chen, S., Jiang, C., Xie, N., Zheng, X., Wang, Y., *et al.* (2019) The genome of the medicinal plant *Andrographis paniculata* provides insight into the biosynthesis of the bioactive diterpenoid neoandrographolide. *Plant J.* **97**, 841–857
44. Cherukupalli, N., Divate, M., Mittapelli, S. R., Khareedu, V. R., and Vudem, D. R. (2016) De novo assembly of leaf transcriptome in the medicinal plant *Andrographis paniculata*. *Front. Plant Sci.* **7**, 1203
45. Gachon, C. M., Langlois-Meurinne, M., and Saindrenan, P. (2005) Plant secondary metabolism glycosyltransferases: The emerging functional analysis. *Trends Plant Sci.* **10**, 542–549
46. Fellenberg, C., Corea, O., Yan, L. H., Archinuk, F., Piirtola, E. M., Gordon, H., Reichelt, M., Brandt, W., Wulff, J., Ehlting, J., and Peter, Constabel, C. (2020) Discovery of salicyl benzoate UDP-glycosyltransferase, a central enzyme in poplar salicinoid phenolic glycoside biosynthesis. *Plant J.* **102**, 99–115
47. Stucky, D. F., Arpin, J. C., and Schrick, K. (2015) Functional diversification of two UGT80 enzymes required for steryl glucoside synthesis in Arabidopsis. *J. Exp. Bot.* **66**, 189–201
48. Jackson, R. G., Lim, E. K., Li, Y., Kowalczyk, M., Sandberg, G., Hoggett, J., Ashford, D. A., and Bowles, D. J. (2001) Identification and biochemical characterization of an Arabidopsis indole-3-acetic acid glucosyltransferase. *J. Biol. Chem.* **276**, 4350–4356
49. Baulcombe, D. C., and Molnar, A. (2004) Crystal structure of p19–a universal suppressor of RNA silencing. *Trends. Biochem. Sci.* **29**, 279–281
50. Wang, H., Wang, C., Fan, W., Yang, J., Appelhagen, I., Wu, Y., and Zhang, P. (2018) A novel glycosyltransferase catalyses the transfer of glucose to glucosylated anthocyanins in purple sweet potato. *J. Exp. Bot.* **69**, 5444–5459
51. Liu, Y., Schiff, M., Marathe, R., and Dinesh-Kumar, S. P. (2002) Tobacco Rar1, EDS1 and NPR1/NIM1 like genes are required for N-mediated resistance to tobacco mosaic virus. *Plant J.* **30**, 415–429
52. Lu, R., Martin-Hernandez, A. M., Peart, J. R., Malcuit, I., and Baulcombe, D. C. (2003) Virus-induced gene silencing in plants. *Methods* **30**, 296–303
53. Garg, A., Sharma, S., Srivastava, P., and Ghosh, S. (2021) Application of virus-induced gene silencing in *Andrographis paniculata*, an economically important medicinal plant. *Protoplasma*. https://doi.org/10.1007/s00709-021-01631-3
54. Kumar, S., Stecher, G., Li, M., Knyaz, C., and Tamura, K. (2018) MEGA X: Molecular evolutionary genetics analysis across computing platforms. *Mol. Biol. Evol.* **35**, 1547–1549
55. Sun, G., Putkaradze, N., Bohnacker, S., Jonczyk, R., Fida, T., Hoffmann, T., Bernhardt, R., Härtl, K., and Schwab, W. (2020) Six uridine-diphosphate glycosyltransferases catalyze the glycosylation of bioactive C13-apocarotenols. *Plant Physiol.* **184**, 1744–1761
56. Shao, H., He, X., Achnine, L., Blount, J. W., Dixon, R. A., and Wang, X. (2005) Crystal structures of a multifunctional triterpene/flavonoid glycosyltransferase from *Medicago truncatula*. *Plant Cell* **17**, 3141–3154
57. Heiling, S., Llorca, L. C., Li, J., Gase, K., Schmidt, A., Schäfer, M., Schneider, B., Halitschke, R., Gaquerel, E., and Baldwin, I. T. (2021) Specific decorations of 17-hydroxygeranyllinalool diterpene glycosides solve the autotoxicity problem of chemical defense in *Nicotiana attenuata*. *Plant Cell* **33**, 1748–1770
58. Liu, J., Wang, Z. T., and Ge, B. X. (2008) Andrograpanin, isolated from *Andrographis paniculata*, exhibits anti-inflammatory property in lipopolysaccharide-induced macrophage cells through down-regulating the p38 MAPKs signaling pathways. *Int. Immunopharmacol.* **8**, 951–958
59. Majumdar, M., Dubey, A., Goswami, R., Misra, T. K., and Roy, D. N. (2020) *In vitro* and in silico studies on the structural and biochemical insight of anti-biofilm activity of andrograpanin from *Andrographis paniculata* against *Pseudomonas aeruginosa*. *World J. Microbiol. Biotechnol.* **36**, 143
60. Zi, J., Mafu, S., and Peters, R. J. (2014) To gibberellins and beyond! Surveying the evolution of (di)terpenoid metabolism. *Annu. Rev. Plant Biol.* **65**, 259–286
61. Zerbe, P., Rodriguez, S. M., Mafu, S., Chiang, A., Sandhu, H. K.,, O'Neil-Johnson, M., Starks, C. M., and Bohlmann, J. (2015) Exploring diterpene metabolism in non-model species: Transcriptome-enabled discovery and functional characterization of labda-7,13E-dienyl diphosphate synthase from *Grindelia robusta*. *Plant J.* **83**, 783–793
62. Heskes, A. M., Sundram, T. C. M., Boughton, B. A., Jensen, N. B., Hansen, N. L., Crocoll, C., Cozzi, F., Rasmussen, S., Hamberger, B., Hamberger, B., Staerk, D., Møller, B. L., and Pateraki, I. (2018) Biosynthesis of bioactive diterpenoids in the medicinal plant *Vitex agnus-castus*. *Plant J.* **93**, 943–958
63. Ding, Y., Murphy, K. M., Poretsky, E., Mafu, S., Yang, B., Char, S. N., Christensen, S. A., Saldivar, E., Wu, M., Wang, Q., Ji, L., Schmitz, R. J., Kremling, K. A., Buckler, E. S., Shen, Z., *et al.* (2019) Multiple genes recruited from hormone pathways partition maize diterpenoid defences. *Nat. Plants* **5**, 1043–1056
64. Sun, Y., Chen, Z., Li, J., Li, J., Lv, H., Yang, J., Li, W., Xie, D., Xiong, Z., Zhang, P., and Wang, Y. (2018) Diterpenoid UDP-glycosyltransferases from Chinese sweet tea and ashitaba complete the biosynthesis of rubusoside. *Mol. Plant* **11**, 1308–1311
65. Misra, R. C., Maiti, P., Chanotiya, C. S., Shanker, K., and Ghosh, S. (2014) Methyl jasmonate-elicited transcriptional responses and pentacyclic triterpene biosynthesis in sweet basil. *Plant Physiol.* **164**, 1028–1044
66. Sandeep, Misra, R. C., Chanotiya, C. S., Mukhopadhyay, P., and Ghosh, S. (2019) Oxidosqualene cyclase and CYP716 enzymes contribute to triterpene structural diversity in the medicinal tree banaba. *New Phytol.* **222**, 408–424

67. Misra, R. C., Sharma, S., Sandeep, Garg, A., Chanotiya, C. S., and Ghosh, S. (2017) Two CYP716A subfamily cytochrome P450 monooxygenases of sweet basil play similar but nonredundant roles in ursane- and oleanane-type pentacyclic triterpene biosynthesis. *New Phytol.* **214**, 706–720
68. Kumar, A., Srivastava, P., Srivastava, G., Sandeep, Kumar, N., Chanotiya, C. S., and Ghosh, S. (2021) BAHD acetyltransferase contributes to wound-induced biosynthesis of oleo-gum resin triterpenes in *Boswellia*. *Plant J.* https://doi.org/10.1111/tpj.15388
69. Bradford, M. M. (1976) A rapid and sensitive method for the quantitation of microgram quantities of protein utilizing the principle of protein-dye binding. *Anal. Biochem.* **72**, 248–254
70. Nakagawa, T., Suzuki, T., Murata, S., Nakamura, S., Hino, T., Maeo, K., Tabata, R., Kawai, T., Tanaka, K., Niwa, Y., Watanabe, Y., Nakamura, K., Kimura, T., and Ishiguro, S. (2007) Improved gateway binary vectors: High-performance vectors for creation of fusion constructs in transgenic analysis of plants. *Biosci. Biotechnol. Biochem.* **71**, 2095–2100
71. Weigel, D., and Glazebrook, J. (2006) Transformation of *Agrobacterium* using the freeze-thaw method. *CSH. Protoc.* **2006**. pdb.prot4666
72. Mageroy, M. H., Jancsik, S., Man, Saint, Yuen, M., Fischer, M., Withers, S. G., Paetz, C., Schneider, B., Mackay, J., and Bohlmann, J. (2017) A conifer UDP-sugar dependent glycosyltransferase contributes to acetophenone metabolism and defense against insects. *Plant Physiol.* **175**, 641–651
73. Kumar, S., Dhanani, T., and Shah, S. (2014) Extraction of three bioactive diterpenoids from *Andrographis paniculata*: Effect of the extraction techniques on extract composition and quantification of three andrographolides using high-performance liquid chromatography. *J. Chromatogr. Sci.* **52**, 1043–1050
74. Shah, S. A., Rathod, I. S., Suhagia, B. N., Pandya, S. S., and Parmar, V. K. (2008) A simple high-performance liquid chromatographic method for the estimation of boswellic acids from the market formulations containing *Boswellia serrata* extract. *J. Chromatogr. Sci.* **46**, 735–738
75. Liang, Z., Jiang, Z., Fong, D. W., and Zhao, Z. (2009) Determination of oleanolic acid and ursolic acid in *Oldenlandia diffusa* and its substitute using high performance liquid chromatography. *J. Food Drug Anal.* **17**, 69–77
76. Srivastava, G., Sandeep, Garg, A., Misra, R. C., Chanotiya, C. S., and Ghosh, S. (2020) Transcriptome analysis and functional characterization of oxidosqualene cyclases of the arjuna triterpene saponin pathway. *Plant Sci.* **292**, 110382
77. Shu, Y., Mannem, C., Xu, G., Gorityala, S., Liu, X., and Xu, Y. (2020) Untargeted metabolomics profiling and global semi-quantitation of a prescription Chinese herbal medicine formula yinqiaosanusing UPLC-QTOF-MS with a single exogenous reference internal standard. *Planta Med. Int.* **7**, e45–e57